CHAPTER 1: INTRODUCTION AND BACKGROUND

1.1 Introduction and Scope

Degeneration of lumbar intervertebral discs is a widespread and unavoidable affliction that will affect almost all people with varying degrees of severity (Garfin and Herkowitz, 1996b). It is strongly implicated as a cause of low back pain, a condition from which 70 to 85 percent of people will suffer at some point during their lifetime (Andersson, 1999). Degeneration is characterised by progressive biochemical and structural changes to the disc extracellular matrix. Comprehensive descriptions of the structural and functional inter-relationships within this matrix are therefore critical to understanding the degenerative process and developing effective treatments.

In the anulus fibrosus, the extracellular matrix has a complex, hierarchical architecture comprised of collagens, proteoglycans, and elastic fibres. Elastic fibres are critical constituents of dynamic biological structures that functionally require elasticity and resilience, however, understanding of their distribution and function in the anulus fibrosus is currently limited. The overall objective of the studies described in this thesis, therefore, was to provide improved experimental descriptions of both the structure and function of the anulus fibrosus elastic fibre network.

In Chapter 1, the intervertebral disc is reviewed with respect to anatomy, biochemistry and microstructure. The mechanical behaviour of the anulus fibrosus is then described, initially in the context of the complete motion segment, then at the tissue level, with a particular focus on tensile anisotropy and heterogeneity. Degeneration of the disc is reviewed in the context of the associated biochemical and structural changes, as are the alterations to mechanical behaviour which occur as a consequence. An overview of elastic fibres is then presented, including biochemistry, distribution

in the anulus fibrosus, their functional roles in composite dynamic biological tissues and their roles in tissue aging and degradation. Elements of the literature are reviewed further, particularly with regard to experimental techniques, in each relevant chapter. Chapter 1 concludes with a statement of the specific objectives of each of the experimental studies subsequently undertaken.

Chapter 2 provides a concise outline of the methods used to obtain cadaveric intervertebal discs for the experimental investigations, and the techniques used to assess degenerative condition.

In Chapter 3, an histological investigation into the structure of the anulus fibrosus elastic fibre network is described. Using novel imaging techiques, the arrangement of elastic fibres was examined with respect to distinct levels of the collagen structural hierarchy, at a level of detail not previously achieved. Additionally, variations in the density of elastic fibres within anulus lamellae were quantitatively investigated with respect to radial and circumferential position.

In Chapter 4, two experimental studies are described which examined the nature of the structure-function associations between elastic fibres and collagen in the context of the distinct structural mechanisms which facilitate tensile deformation. In the first of these studies, the effect of enzymatically removing elastic fibres on the passive behaviour of collagen fibre planar crimp was qualitatively examined. In the second study, the hypothesis that elastic fibres provide both intralamellar and interlamellar cross-connectivity was examined by subjecting anulus fibrosus specimens to radial strains, then histologically examining the patterns of elastic fibre rearrangement both within collagen bundles and at lamellar interfaces.

In Chapter 5, an investigation into the nature and magnitude of the contribution made by elastic fibres to the tissue-level, quasi-static, tensile mechanical properties of the anulus fibrosus is described. Using a combination of biochemically validated enzymatic treatments and uniaxial biomechanical tests, changes to elastic modulus and extensibility following selective removal of elastic fibres were investigated. Separate enzymatic treatments and mechanical tests were used to account for the likely effects of non-specific glycosaminoglycan degradation. The dependance of mechanical properties on circumferential position in the disc and degenerative condition was also examined.

Finally, Chapter 6 contains a summary of major findings and their implications, and a discussion of potential future investigations.

1.2 Background

1.2.1 The Intervertebral Disc

1.2.1.1 Anatomy

Intervertebral discs are partially movable joints connecting each of the vertebral bodies in the spine. In the cervical spine discs are roughly elliptical, but further down through the thoracic to the lumbar region, discs become kidney shaped. Disc area also increases progressively with spine level, reflecting changing mechanical roles. The internal structure of each disc, however is very similar at all spine levels (Oegema, 1993). This structure is comprised of three integrated anatomical regions: the highly hydrated nucleus pulposus at the centre; the peripheral, cartilaginous anulus fibrosus; and superiorly and inferiorly, two end plates of hyaline cartilage (Eyre, 1979). This anatomy as it appears in a mid-sagittal cross-section of the disc is illustrated schematically in Figure 1.1.

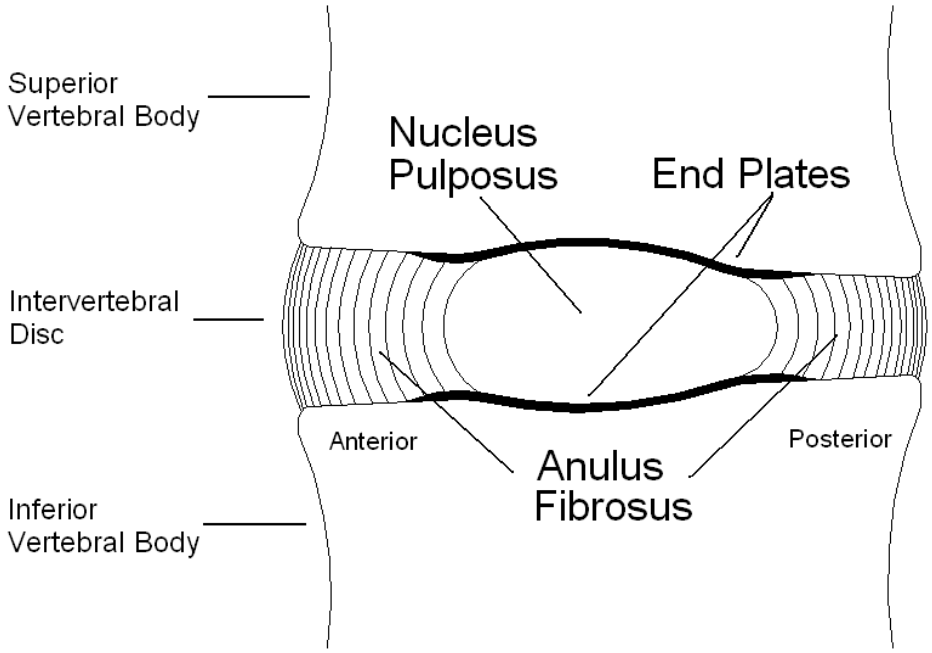


Figure 1.1. The three anatomical regions of the lumbar disc as they appear in a mid-sagittal cross-section.

1.2.1.2 Biochemical Composition

1.2.1.2.1 Extracellular Matrix

Water forms the bulk of the tissue weight in the intervertebral disc, constituting 70 to 82 percent of the nucleus, 65 to 75 percent of the inner anulus and 55 to 65 percent of the outer anulus (Urban, 1996).

Collagens constitute 40-60 percent of the dry weight of the outer anulus, 25-40 percent of the inner anulus and 18-30 percent of the nucleus (Holm, 1996; Urban, 1996). Collagen types I and II are the most prevalent; opposing gradients between these collagen types exist radially from the disc periphery to the nucleus, with the outer anulus consisting almost entirely of type I and the nucleus containing exclusively type II (Eyre and Muir, 1976). Collagen types III, V, VI, IX and XI are also present in minor quantities (Oegema, 1993; Urban, 1996). The predominant intermolecular crosslinking amino acid of collagen in the intervertebral discs is hydroxylysylpyridinoline (pyridinoline) (Pokharna and Phillips, 1998). The concentration of pyridinoline crosslinks in the human disc is higher than any other connective tissue (Pokharna and Phillips, 1998). Crosslink concentration in the disc is heterogeneous, increasing from the outer anulus to the nucleus (Duance *et al.*, 1998).

Proteoglycans represent the second most prevalent constituent of the disc in terms of dry weight after collagen (Urban, 1996). Proteoglycan concentration is highest in the nucleus, constituting approximately 50 percent of the dry weight, compared with around 15 percent in the anulus. A increasing gradient in proteoglycan concentration exists from the anulus periphery to the transition zone (Eyre, 1979; Urban, 1996).

The major proteoglycan of the disc is aggrecan. Attached to each aggrecan core protein are approximately 100 chondroitin sulphate and 30 keratan sulphate glycosaminoglycan side chains (Feng *et al.*, 2006). The ratio of keratan sulphate to chondroitin sulphate in the disc is higher than in other tissues (Eyre, 1979). Aggrecan commonly aggregates by attaching via link proteins to long chains of hyaluronan. Small proteoglycans, including decorin, biglycan and fibromodulin are also present (Oegema, 1993). Proteoglycans such as aggrecan control tissue hydration by generating osmotic pressure and resisting fluid loss under compressive stresses, and are thus critical to the correct mechanical function of the disc (Holm, 1996). This osmotic pressure arises from the fixed negative charges attributable to the polyelectrolytic nature of the glycosaminoglycans (Urban, 1996).

The balance of the extracellular matrix is comprised of additional glycoproteins, lipids and elastic fibres (Eyre, 1979; Holm, 1996). The elastic fibre content of the disc is described in detail in section 1.2.2.1.

1.2.1.2.2 Cellular Component

Cell density in the disc is relatively low compared with other connective tissues (9000/mm^3 in the anulus fibrosus compared with 15000/mm^3 in articular cartilage) (Maroudas *et al.*, 1975). Cell density is highest in the outer anulus and in the end plates, and lowest in the nucleus (Maroudas *et al.*, 1975). Cell types vary with region: the anulus and nucleus contain a mixture of chondrocytes and fibrocytes; the end plates contain mainly chondrocytes (Holm, 1996). Regional variations in the cellular matrix across the anulus fibrosus of bovine discs have been described in detail (Bruehlmann *et al.*, 2002). Within the outer lamellae, fusiform cells with processes up

to 60μm long are aligned parallel to the collagen fibres. The cell processes link together to form interconnections between adjacent cells. It has been theorised that these processes facilitate both the sensing of mechanical strains and intercellular communication. In the inner anulus, cells are more rounded, but still have extensive processes. Unlike those in the outer anulus they appeared to have no preferential alignment, and maintain only limited intercellular linkages. The cell population of the inter-lamellar regions is distinct from that found within lamellae. Cells in these regions have a flattened, disc-shaped morphology, and multi-directional processes, except those between the outermost lamellae, which are devoid of processes (Bruehlmann *et al.*, 2002).

Figure 1.2 illustrates different cell morphologies in the outer anulus fibrosus of a sixteen year-old L3-L4 human disc, including fusiform cells (F) within a lamella and disc-shaped cells (D) at the lamellar boundaries.

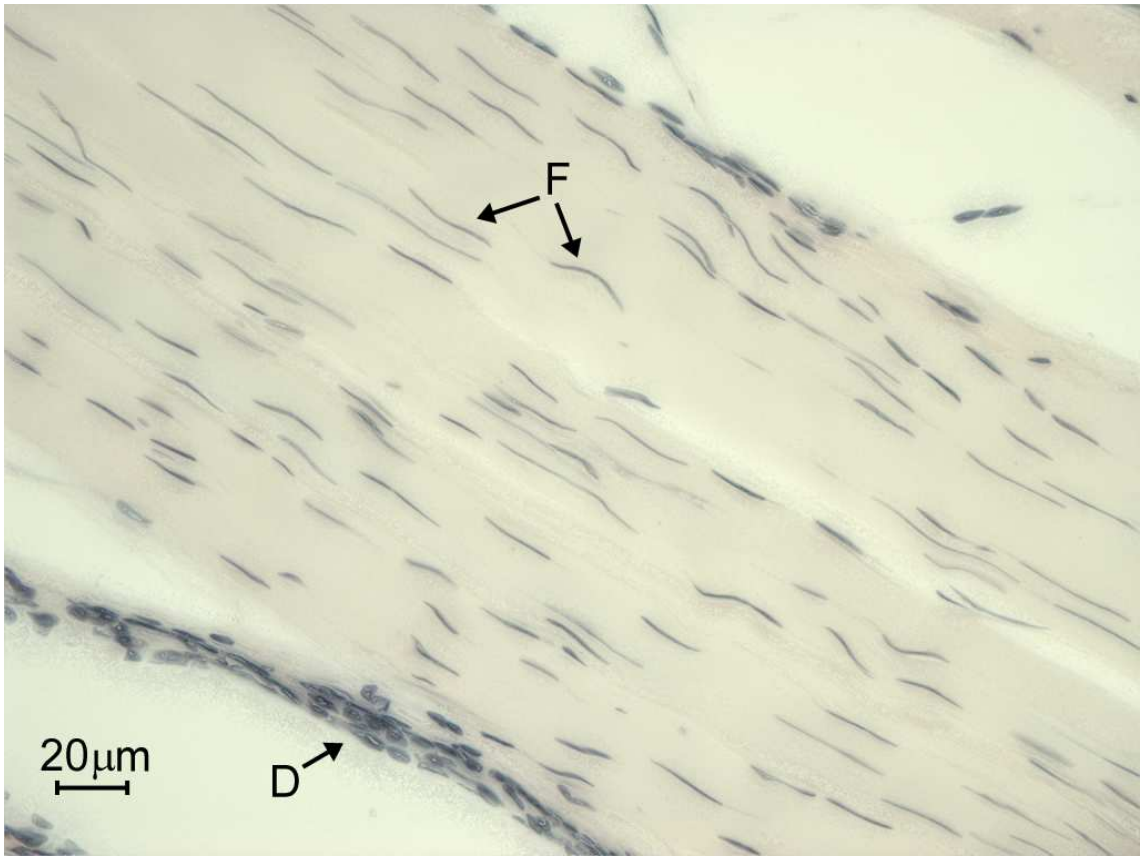


Figure 1.2. Cells in the outer anulus of a 16 year old L3-L4 human disc. Those within a lamella are fusiform (F), while those at the lamella boundary are disc-shaped (D) (author's image, haematoxylin and eosin stain, transverse-plane section, 40 times objective magnification).

1.2.1.3 Microstructure

The nucleus pulposus is composed of an irregular meshwork of type II collagen fibrils, approximately 20 to 50 nm in diameter (Eyre, 1979; Holm, 1996). At the transition zone, these fibrils subtly merge with the collagen bundles of the anulus lamellae; they are not directly connected to the end plate surfaces (Urban, 1996). The collagen meshwork is embedded in an hydrated ground matrix rich in proteoglycans (Eyre, 1979).

The two end plates superior and inferior to the disc are comprised of a thin layer of hyaline cartilage with a non-uniform average thickess of approximately 0.6 mm, thinnest proximal to the nucleus (Roberts *et al.*, 1989). On the side adjacent to the disc, the end plates merge and integrate tangentially with the collagen fibres of the anulus; on the opposing side the end plates integrate with the vertebral cortex (Szirmai, 1970).

In the anulus fibrosus, the most important structural elements are bundles of type I collagen fibrils, arranged in roughly concentric lamellae arround the nucleus pulposus. These bundles are oriented at angles of approximately 30 degrees to the transverse plane of the disc with their directions alternating in each consecutive lamella (Figure 1.3). This angle varies somewhat, from a maximum near the anulus periphery to a minimum closer to the nucleus (Cassidy *et al.*, 1989). In the inner anulus, fibre bundles connect superiorly and inferiorly to the end plates, and in the outer anulus fibres connect directly to the vertebral cortices by way of Sharpey's fibres (Eyre, 1979).

The thickness of the lamellae varies with both circumferential and radial location (Cassidy *et al.*, 1989; Marchand and Ahmed, 1990). The outermost lamellae are thinnest, frequently less than 100μm, and the innermost are the thickest, typically over 250μm. Circumferentially, lamellae are thicker at the anterior and lateral regions than the posterior. Overall, the anulus is thickest, both radially and axially, at the anterior, and thinnest at the posterior. The total number of lamellae between the periphery and the transition zone varies with circumferential location, from a maximum in lateral regions, to significantly less at anterior regions, and to a minimum at the posterior (Marchand and Ahmed, 1990). Despite their superficial macroscopic appearance, lamellae are discontinuous in both the axial and circumferential directions. Circumferentially, around 48 percent of lamellae are discontinuous. The percentage of incomplete lamellae varies significantly with circumferential region, with a maximum occurring posterolaterally (53 percent), and a minimum anteriorly (43 percent) (Marchand and Ahmed, 1990; Tsuji *et al.*, 1993). Two mechanisms of lamellar interruption have been described: firstly, where there are three parallel lamellae, the central lamella terminates, and the outer two continue separately; secondly, where the central lamella terminates, and the outer two merge to form a single lamella (Marchand and Ahmed, 1990).

Collagen bundles are composed of fibrils 0.1 to 0.2 μm in diameter; each bundle is 10 to 15 μm in diameter (Holm, 1996). Anulus collagen fibres display a characteristic planar crimp, the angle and period of which vary with radial position. Crimp angle increases inward from the periphery to the transition zone, whereas the period decreases over the same distance; crimp length however remains constant (Cassidy *et al.*, 1989).

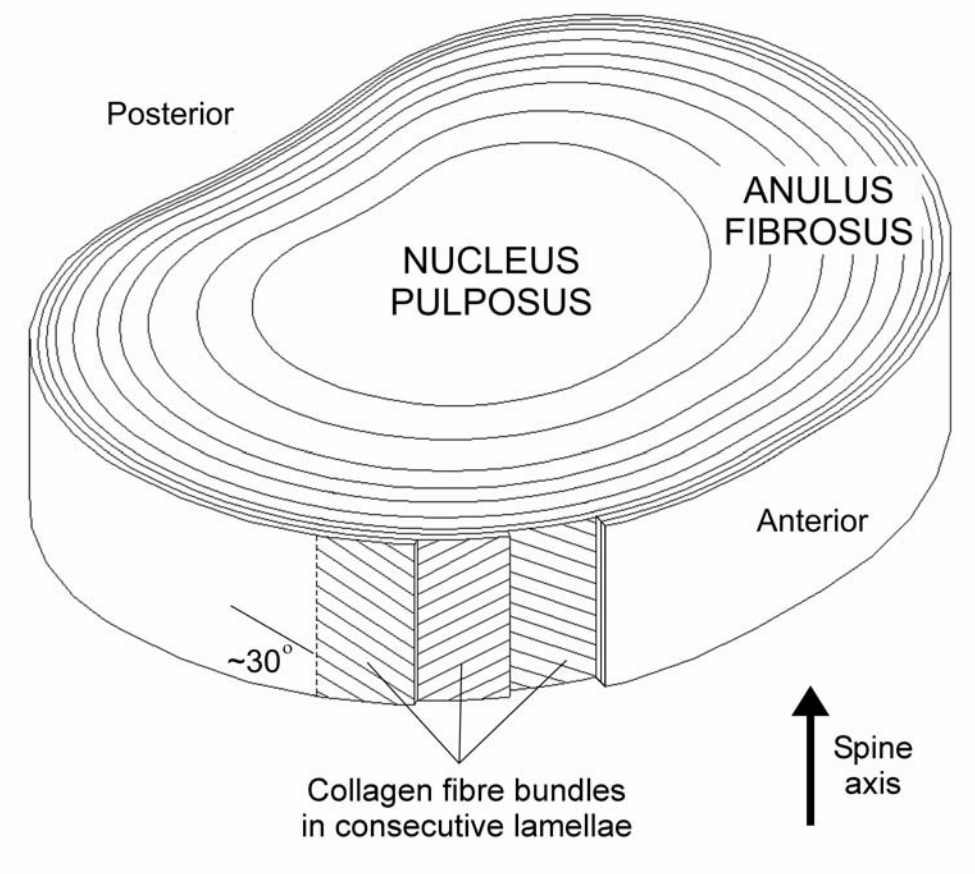


Figure 1.3. Three-dimensional representation of the intervertebral disc illustrating the concentric lamellar structure and alternating collagen fibre bundle orientations in the anulus fibrosus.

The nature of the hierarchical microstructure present within individual anulus collagen fibre bundles was recently described (Pezowicz *et al.*, 2005). In bundles stretched parallel to the collagen fibre direction, the mechanism of deformation is characterised by progressive uncrimping of fibrous elements, and re-crimping once the applied load is released. In contrast, when stretched perpendicular to the collagen fibre direction, complex arrays of interconnecting fibrous linkages are revealed, demonstrating a high level of structural integration perpendicular to the predominant collagen fibre direction (Figure 1.4). Multiple mechanisms of interconnection exist with respect to these elements, including both single and bi-directional cross-over elements, and splitting and sub-splitting of those elements.

The structural basis of cohesion between collagen bundles in consecutive and non-consecutive lamellae, has also recently been described (Pezowicz *et al.*, 2006a). Figure 1.5A shows in-plane and cross-sectioned bundles in consecutive lamellae in an undeformed anulus fibrosus specimen. When subjected to loads perpendicular to the plane containing the collagen fibres, deformation occurs by way of transverse bundle elongation and interlamellar separation (Figure 1.5B). As lamellae separate, a highly developed system of linking elements is revealed connecting adjacent bundles (Figure 1.5C). Additionally, complex bridging elements are present, passing between the collagen bundles of one lamella to directly connect bundles in non-consecutive lamellae (Figure 1.5D).

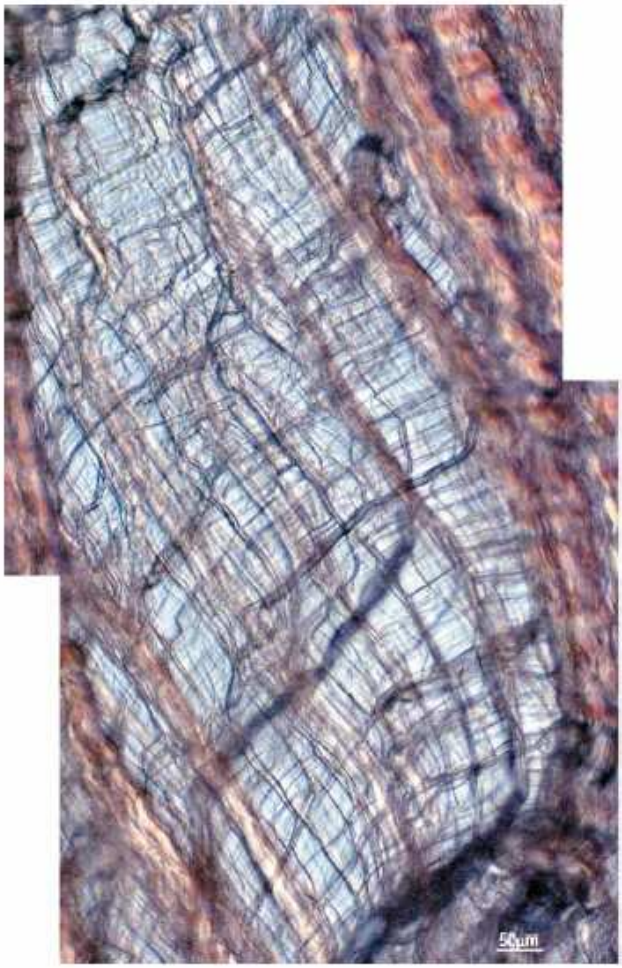


Figure 1.4. A collagen bundle subjected to deformation perpendicular to the collagen fibre direction, illustrating the complex mechanisms of transverse structural integration (adapted from (Pezowicz *et al.*, 2005)).

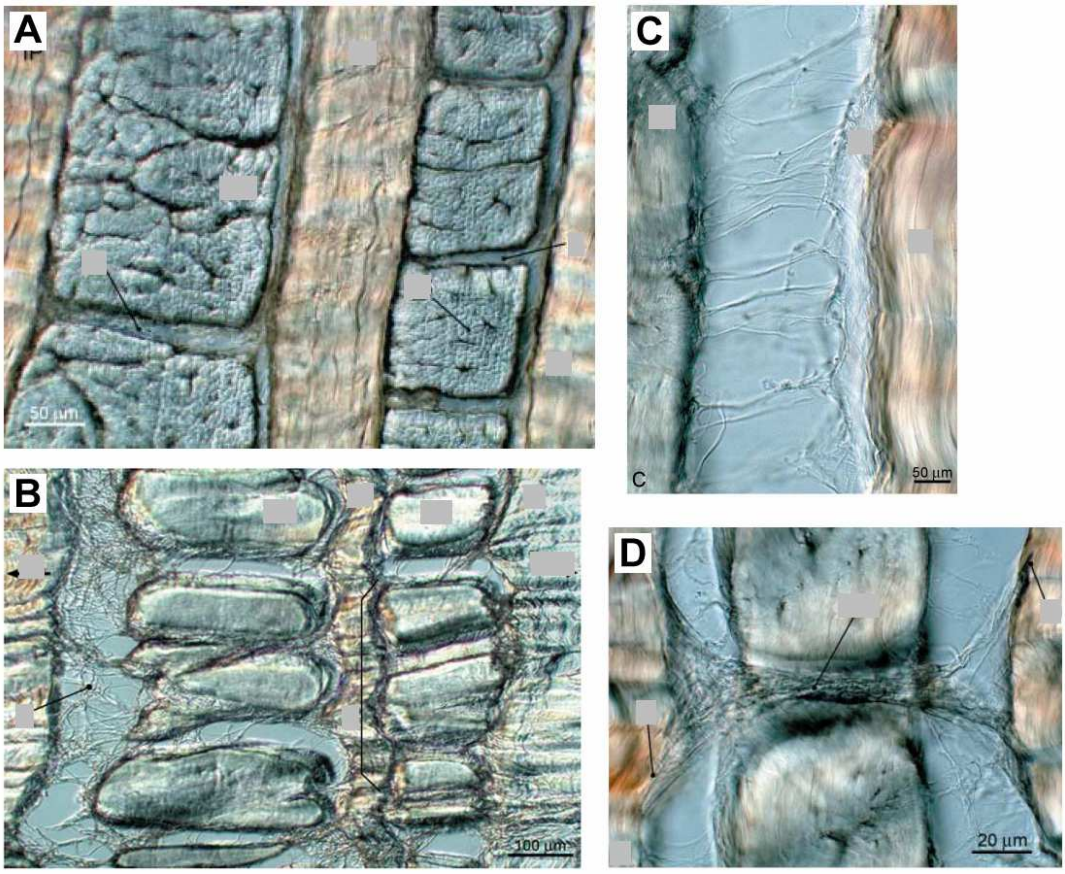


Figure 1.5. A. In-plane and cross-sectioned collagen bundles in consecutive lamellae in the anulus fibrosus. B. Lamellae subjected to transverse deformation resulting in bundle elongation and lamellar separation. C. Linking elements connecting consecutive lamellae undergoing transverse separation. D. A 'bridging element' passes between two collagen bundles to connect non-consecutive lamellae (adapted from (Pezowicz *et al.*, 2006a), original annotations masked).

1.2.1.4 Mechanical Properties

1.2.1.4.1 Motion Segment

Anatomically each motion segment represents an elementary component of the spine, being comprised of a single intervertebral disc, superior and inferior vertebral bodies, ligaments and zygapophyseal joints. In the context of each motion segment, the mechanical role of the intervertebral disc is two-fold: to transmit and distribute compressive forces down the spine; and to provide mobility in the form of flexion, extension, lateral bending, axial torsion, and complex combinations of these modes (Langrana *et al.*, 1996).

In compression, the central nucleus expands radially, contained superiorly and inferiorly by the endplates, and peripherally by the anulus fibrosus, generating a region of constant hydrostatic pressure across the disc (Figure 1.6) (McNally and Adams, 1992; Adams *et al.*, 1996). Consequentially, the anulus fibrosus experiences tensile circumferential strains and compressive radial strains in all regions (Table 1.1 and Table 1.2) (Tsantrizos *et al.*, 2005). While pure compression results in nuclear expansion alone, bending results in nuclear expansion and migration: in flexion, the nucleus migrates to the posterior; in extension the nucleus migrates to the anterior; in lateral bending the nucleus migrates contra-laterally. Nuclear migration subjects opposite sides of the anulus to radial tensile strains and radial compressive strains respectively (Table 1.1), and all regions of the anulus to circumferential tensile strains (Table 1.2) (Tsantrizos *et al.*, 2005).

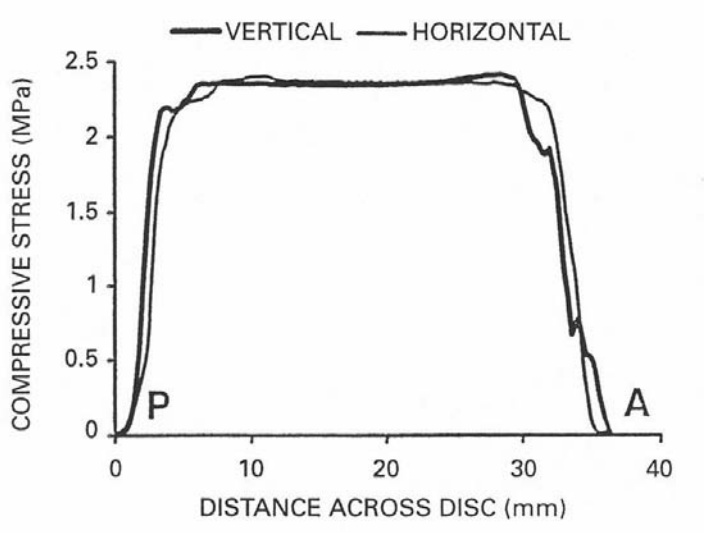


Figure 1.6. The internal pressure profile of a non-degenerate intervertebral disc under pure axial compression (Adams *et al.*, 1996).

In flexion, the posterior anulus experiences positive axial strains of up to 60 percent and the anterior anulus experiences negative axial strains of up to 35 percent. In extension, the anterior anulus experiences positive axial strains of up to 30 percent and the posterior anulus experiences negative axial strains of up to 26 percent (Pearcy and Tibrewal, 1984).

Circumferential and axial tensile deformation of the anulus is able to occur as a result of both collagen fibre extension and reorientation of those fibres relative to one another. During compression, the tilt angle of the collagen fibres relative to the transverse plane decreases (Klein and Hukins, 1982a). In torsion, the tilt angle of fibres with positive slope relative to the rotation direction decreases and the tilt angle of fibres with negative slope relative to the rotation direction decreases; in bending, tilt angle on the contralateral side increases, and decreases on the opposite side (Klein and Hukins, 1982b).

Tensile strains occur within anulus collagen fibre bundles parallel to their principle stress axes in compression due to radial bulge, on the contra-lateral side during bending, and during axial torsion (Stokes, 1987). The magnitudes of these strains under each of these loading conditions, measured on the exterior surface of the anulus, are summarised in Table 1.3. Finite element models predict that the greatest collagen fibre bundle strains occur in the posterolateral regions of the anulus under complex physiological loading, such as, lateral bending combined with axial torsion (Schmidt *et al.*, 2007).

Internal shear strains under physiological loading conditions are greatest in the posterolateral region of the anulus during lateral bending, and in the anterior and anterolateral regions during flexion (Costi *et al.*, 2007).

NOTE: This table is included on page 21 in the print copy of the thesis held in the University of Adelaide Library.

Table 1.1. Internal radial strains (percent) experienced by the non-degenerate annulus fibrosus under physiological loading (Tsantrizos *et al.*, 2005). Positive = tensile; negative = compressive.

NOTE: This table is included on page 21 in the print copy of the thesis held in the University of Adelaide Library.

Table 1.2. Internal circumferential strains (percent) experienced by the non-degenerate anulus fibrosus under physiological loading (Tsantrizos *et al.*, 2005). Positive = tensile; negative = compressive.

Region	**Compression***	**Flexion****	**Extension****	**Torsion****[†]
Anterior	+1.73	+0.07	+0.59	-0.44
Posterolateral	+1.66	+0.27	+0.51	-0.94

Table 1.3. Collagen fibre bundle strains on the exterior surface of the anulus fibrosus under various loading conditions (disc only) (Stokes, 1987). *Percent; **percent per degree; [†]strains positive (tensile) for torsion in the opposite direction.

1.2.1.4.2 Tissue Level

Excised specimens of anulus fibrosus tissue tested at any orientation display a quasi-static tensile stress-strain response typical of soft biological tissues (Figure 1.7) (Fung, 1981). This response begins with an approximately linear ‘toe’ region, the slope of which will be referred to in this thesis as *initial elastic modulus*; a region of non-linear transition then ensues corresponding approximately to a strain which will be referred to as the *extensibility*, and which is typically representative of the progressive re-alignment of fibrous elements along the axis of the applied strain, uncrimping of fibrillar collagens and redistribution of the fluid phase; the response then displays a second, higher strain linear region, the slope of which will be referred to as the *ultimate elastic modulus*; beyond this the response encounters a yield strain, a period of plasticity, an ultimate strain and finally, a failure strain.

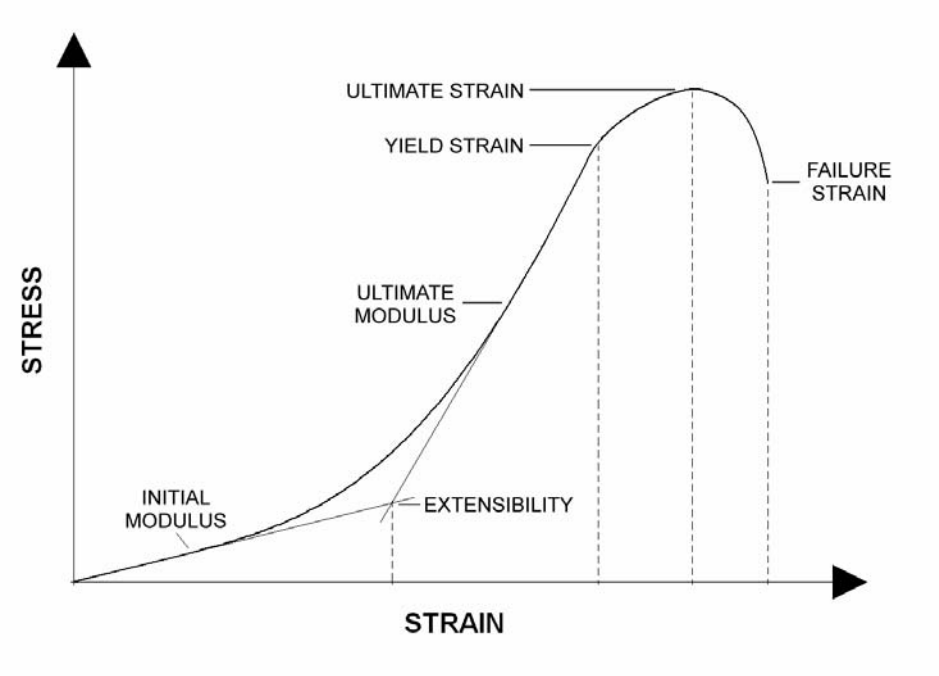
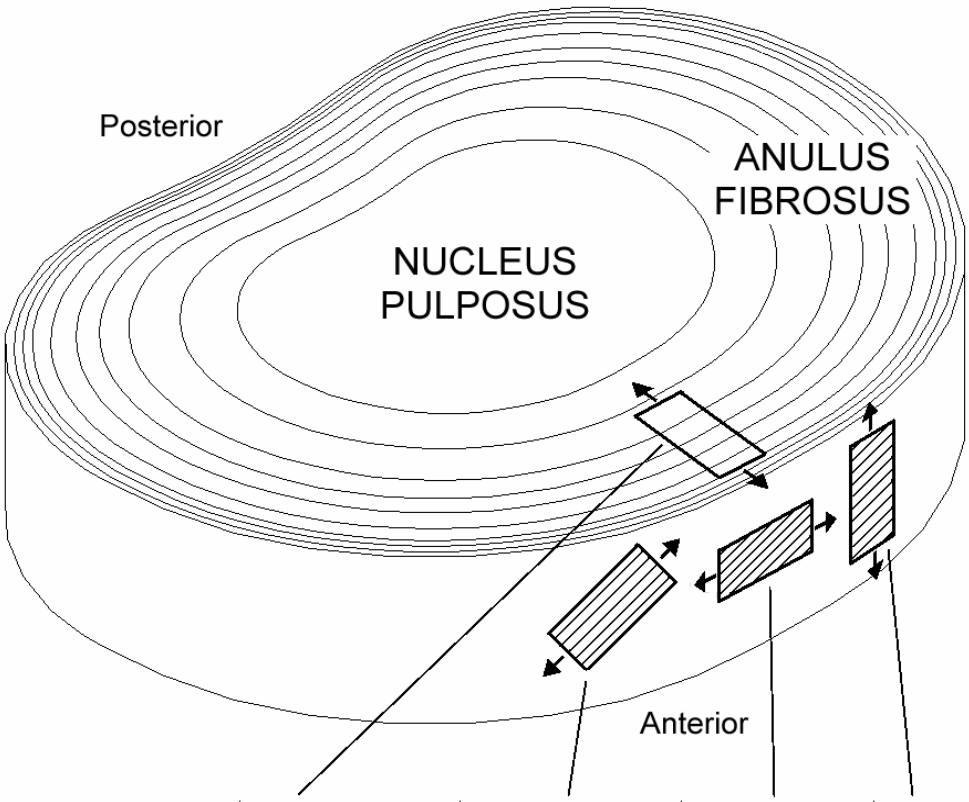


Figure 1.7. Components of the quasi-static stress-strain response which is typical of anulus fibrosus tissue specimens tested in unaxial tension.

The hierarchical microarchitecture of the anulus fibrosus that serves to provide the motion segment with its unique functional abilities results in extensive tissue level anisotropy with respect to its quasi-static tensile mechanical response. The seminal study of Galante demonstrated that these properties reflect a direct relationship between the test orientation and the principal direction of the collagen fibre bundles (Galante, 1967). This important structure-function relationship has been confirmed and developed further in many subsequent studies. With reference to Figure 1.8, both initial elastic modulus and ultimate elastic modulus are smallest in the radial direction, transverse to the plane of the lamellae (Marchand and Ahmed, 1989; Fujita *et al.*, 1997; Elliott and Setton, 2001). For a single lamella, initial modulus and ultimate modulus are greatest along the axis parallel to the direction of the collagen fibre bundles, and weakest transverse to this direction (Skaggs *et al.*, 1994; Holzapfel *et al.*, 2004). For multilamellar specimens, ultimate modulus is an order of magnitude larger (Marchand and Ahmed, 1989). In the axial and circumferential orientations, mechanical properties fall between these two extremes, with both initial modulus and ultimate modulus approximately one order of magnitude greater in the circumferential than the axial direction (Acaroglu *et al.*, 1995; Elliott and Setton, 2001). The Poisson's ratio of the anulus, defined as the ratio of deformation transverse to the direction of the applied strain to the deformation parallel to the direction of the applied strain, is also anisotropic. In the radial direction, the Poisson's ratio is less than unity, reflecting minimal relative transverse deformation. In contrast, in the circumferential direction, the Poisson's ratio exceeds unity, reflecting greater relative transverse deformation (Elliott and Setton, 2001).



	Radial	Collagen Bundle	Circumferential	Axial
Initial Modulus:	0.19[a], 0.19[b]	3.5[d]	2.11[a]	0.30[a]
Ultimate Modulus:	0.45[a], 0.47[b], 0.16[c]	87.5[e], 43[d]	11.53[a], 25[f]	0.89[a]

[a] Elliott and Setton, 2001
[b] Fujita *et al.*, 1997
[c] Marchand and Ahmed, 1989
[d] Holzapfel *et al.*, 2004
[e] Skaggs *et al.*, 1994
[f] Ebara *et al.*, 1996

Figure 1.8. Anulus fibrosus specimens tested at different orientations demonstrate significant mechanical anisotropy. (In some cases mean values have been estimated from multiple data and graphs in the publications cited). Units are MPa.

In addition to displaying anisotropy, mechanical properties are heterogeneous with both circumferential and radial position in the disc. The extent of this heterogeneity varies with orientation. Parallel to the direction of the collagen fibre bundles, ultimate elastic modulus is significantly higher in the outer lamellae than the inner lamellae, but initial modulus is not (Skaggs *et al.*, 1994; Holzapfel *et al.*, 2004). There is conflicting evidence as to whether ultimate modulus in this orientation is dependant on circumferential position: one study has found significantly higher values for anterior specimens (Skaggs *et al.*, 1994); a more recent study found no such dependence (Holzapfel *et al.*, 2004). Initial modulus parallel to the collagen fibre bundles is circumferentially homogeneous (Holzapfel *et al.*, 2004), failure stress is higher in the anterior regions and failure strain higher in the posterolateral regions (Skaggs *et al.*, 1994).

In the circumferential orientation ultimate elastic modulus, failure stress and strain energy density are all significantly greater in the outer anulus (Acaroglu *et al.*, 1995; Ebara *et al.*, 1996; Elliott and Setton, 2001). Failure strain and Poisson's ratio are greater in the inner anulus (Acaroglu *et al.*, 1995). Initial modulus shows no significant dependence on radial position (Elliott and Setton, 2001). Ultimate modulus, strain energy density and failure stress all display circumferential heterogeneity, being higher anteriorly than posteriorly, however failure strain and Poisson's ratio do not (Acaroglu *et al.*, 1995). In the axial orientation, neither initial modulus nor ultimate modulus display radial heterogeneity, however Poisson's ratios are significantly greater in the inner anulus (Elliott and Setton, 2001). Axially oriented specimens tested with sections of adjacent vertebral bodies attached display significant circumferential heterogeneity, with both ultimate elastic modulus and

failure stress significantly higher in the posterior regions of the anulus than the anterior (Green *et al.*, 1993). Mechanical properties in the radial orientation exhibit limited radial heterogeneity, with ultimate modulus and ultimate strain significantly greater and lower respectively in the middle anulus than the inner and the outer, but no significant circumferential heterogeneity (Fujita *et al.*, 1997).

In contrast to tension, the tissue-level compressive mechanical properties of the anulus display only minimal heterogeneity and no anisotropy (Best *et al.*, 1994; Iatridis *et al.*, 1998). For radially orientated specimens, compressive modulus displays a trend to be higher in the middle and outer anulus compared to the inner anulus, but circumferentially is homogeneous (Best *et al.*, 1994).

The shear mechanical properties of the anulus fibrosus at the tissue level display both heterogeneity and anisotropy. Shear modulus is significantly greater for axially oriented specimens than for circumferentially oriented specimens. In the axial orientation, modulus increases with distance form the transition zone, and in the circumferential orientation, modulus is significantly greater in the outer anulus than the middle anulus (Fujita *et al.*, 2000).

The hydraulic permeability of the anulus, measured in the posterolateral region, displays significant anisotropy, being greatest in the radial orientation and lowest in the circumferential orientation (Gu *et al.*, 1999).

While much of the mechanical anisotropy of the anulus fibrosus can be attributed to the structural complexity of the collagen fibre matrix, the structural and biochemical sources of heterogeneity are less clear. Compressive modulus and permeabililty show

dependance on both tissue hydration and glycosaminoglycan concentration (Best *et al.*, 1994; Perie *et al.*, 2006b). The radial heterogeneity of the concentrations of both these consituents may therefore partially explain the observed variability in this spatiality with respect to the first of these (Best *et al.*, 1994; Urban, 1996).

An examination of correlations between the tensile behaviour of anulus specimens oriented parallel to the direction of the collagen fibre bundles and biochemical composition found a weak negative correlation between modulus and hydration, but no significant relationships between either collagen or glycosaminoglycan content, and any mechanical properties (Skaggs *et al.*, 1994).

To date there have been no studies published which have examined correlations between matrix composition and tensile mechanical behaviour in the circumferential, axial or radial orientations. Taken in the context of the mechanisms of deformation outlined in sections 1.2.1.3 and 1.2.1.4.1, particularly with respect to both collagen bundle expansion and lamellar separation in radial tension, and relative collagen fibre bundle reorientation in axial and circumferential tension, the mechanical roles of non-collagenous constituents are potentially very important. Structure-function analytical models of anulus behaviour support this contention (Elliott and Setton, 2001; Guerin and Elliott, 2007).

1.2.1.5 Degeneration and Aging

There is considerable debate as to the strength of the connections that exist between disc degeneration and low back pain in general. The aetiology of low back pain is still poorly understood, and there are several structures in the spine other than the disc which have been implicated as causes (Garfin and Herkowitz, 1996b). The disc is thought to be both a direct and indirect source of pain. Other causes include osteoarthritis (Lewin, 1964), osteoporosis of the vertebral bodies (Hansson and Keller, 1996), spinal fractures (Garfin *et al.*, 1996a), spondylolisthesis (Wiltse and Rothman, 1996) and spinal tumours (Weinstein, 1996). Because the pathogenic changes that occur in the disc generally precede these conditions, it has been suggested that they may act as precursors in some instances and thereby cause back pain indirectly (Garfin and Herkowitz, 1996b).

Innervation in the intervertebral disc is generally small and concentrated in the superficial anulus and end plates (Fagan *et al.*, 2003). As a consequence, back pain does not generally originate in the disc itself. Instead, it results from the impact changes to the disc have on surrounding structures. One of the most striking examples is posterior disc prolapse, a condition that has been found to be present in 15.2 percent of all spines and one that occurs most commonly in the lower lumber region (Schmorl and Junghanns, 1971). In this instance, a section of the posterior or posterolateral anulus ruptures or dissects and disc material bulges or escapes into the spinal canal (Vernon-Roberts, 1988).

Degeneration is known to increase proportionally with age (Garfin and Herkowitz, 1996b). There is a general consensus that this is both due to inherent or genetic factors, and the physical stresses and cumulative defects that occur in the disc during

normal daily activity. Degenerative changes to the disc occurring independent of age may be a result of physiological trauma, or pathologies involving changes to disc chemistry or the surrounding structures (Garfin and Herkowitz, 1996b). It is convenient to define degeneration broadly as those changes which occur to disc structure and chemistry, either pathologically, traumatically or chronologically, which impact negatively on normal disc function. Identifying the nature and precursors of those chemical and structural changes is critical to understanding, preventing and potentially reversing the degenerative process.

1.2.1.5.1 Biochemical Changes

Degeneration of the lumbar disc is accompanied by a marked decrease in proteoglycan content, and in particular, a loss of aggrecan (Buckwalter, 1995; Lipson, 1996; Urban, 1996). Proteoglycan loss is especially prevalent in the nucleus (Buckwalter, 1995; Holm, 1996). Degeneration is also accompanied by an increase in the ratio of keratan sulphate to chondroitin sulphate (Szirmai, 1970; Eyre, 1979). The biological reasons for this decrease in proteoglycans is still poorly understood, however there is evidence that it is due in part to increasing levels of matrix metalloproteinases and aggrecanases, and imbalances between these and their respective tissue inhibitors (Roberts *et al.*, 2000). Changes to collagen in the disc with aging and degeneration also occur. The concentration of pyridinoline crosslinks decreases with both aging and degeneration, where as the concentration of pentosine crosslinks displays the opposite trend. No significant differences have been observed in these parameters between the nucleus and anulus (Pokharna and Phillips, 1998). There also is evidence of age and degeneration related changes in elastin content in both the anulus and nucleus, described in section 1.2.2.4.

1.2.1.5.2 Structural Changes

Structural changes tend to appear first and progress most rapidly in the lumbar spine, and are least prevalent in the thoracic spine. This is likely in part due to the more extensive range of motion and higher compressive loads experienced by lumbar discs. The lowest lumbar discs are the most susceptible to degeneration (Vernon-Roberts, 1988). Degeneration typically begins with a loss of nuclear hydration and the loss of a distinct transition zone between the nucleus and anulus. As degeneration progresses, clefts may appear in the nucleus, then later in the anulus, with those near the disc periphery becoming vascularised and innervated. The anular layers become coarse, and the disc in general appears more fibrous. Anular tears – circumferential, radial and peripheral – may be present, Schmorl's nodes (small herniations of disc material through the end plates extending into the vertebral bodies) may appear, as may peripheral herniations in the most severe cases. On the exterior of the spine, the presence of osteophytes is often a sign that adjacent discs may be degenerate (Holm, 1996). At the ultrastructural level, aged and degenerate discs have been observed to contain collagen fibrils of widened and irregular diameters (Gruber and Hanley, 2002). At the microstructural level, damage to the anulus is commonly manifested as matrix cracking (intra-collagen bundle splitting), delamination and fibre failure (Iatridis and ap Gwynn, 2004). Over-pressurisation, tensile overload and fatigue have each been demonstrated to result directly in such damage (Iatridis *et al.*, 2005; Pezowicz *et al.*, 2006b).

1.2.1.5.3 Mechanical Changes

The magnitude of the internal strains experienced by the disc under physiological loading exhibits dependance on degenerative condition (Tsantrizos *et al.*, 2005).

Radial strains, both tensile and compressive, occuring as a result of nuclear expansion, contraction and migration, increase in magnitude with degeneration in flexion, extension and lateral bending. The magnitude of the circumferential tensile strains in the posterolateral regions of the anulus also increases with degeneration under all loading modalities – those in the anterior regions are greater during extension and lateral bending but smaller during compression and flexion.

The distribution of internal compressive stress also demonstrates dependance on degenerative condition (Adams *et al.*, 1996). Severely degenerated discs have reduced overall internal pressure, with stress peaks occuring in the anterior and posterior regions of the anulus fibrosus. Figure 1.9 shows the internal stress profile of a degenerate disc, which presents clear differences when compared to the profile of a non-degenerate disc (Figure 1.6). There is evidence that minor damage to the vertebral body end plates leads to altered pressure distributions such as those illustrated in Figure 1.9, which in turn lead to progressive structural deterioration such as inward fold of anulus lamellae (Adams *et al.*, 2000).

Changes to motion segment stiffness under multiple loading modalities have been correlated with the severity of the macroscopic alterations in disc structure that occur as degeneration progresses (Thompson *et al.*, 2000). Circumferential tears increase motion segment stiffness in flexion and extension, and decrease torsional stiffness; radial tears increase stiffness in extension; and rim lesions increase flexion stiffness and decrease torsional stiffness. There is also evidence that motion segment stiffness is negatively correlated with level of hydration (Costi *et al.*, 2002).

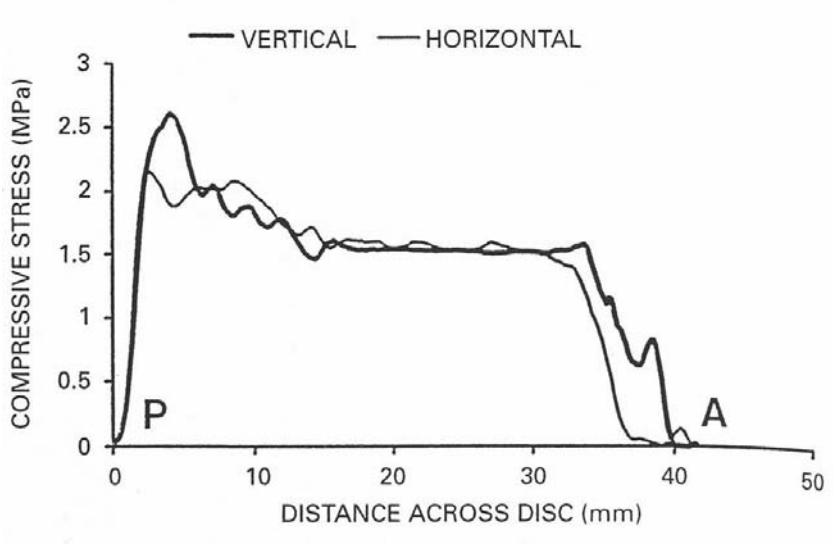


Figure 1.9. The pressure distribution in a degenerate intervertebral disc under pure axial compression (adapted from (Adams *et al.*, 1996)).

At the tissue-level, the mechanical properties of anulus fibrosus demonstrate dependance on age and degenerative condition in tension, compression and shear. In the radial orientation, tissue from moderately degenerate discs displays weakened yield strength and ultimate tensile strength, and increased initial and ultimate modulus compared with non-degenerate discs (Fujita *et al.*, 1997). In the circumferential orientation, Poisson's ratio increases, and tensile yield strength, strain energy density and fibre reorientation decrease with degeneration (Acaroglu *et al.*, 1995; Guerin and Elliott, 2006). Initial modulus is positively correlated with age (Guerin and Elliott, 2006).

Axial and radial specimens tested in confined compression display significantly increased stiffness with increasing degenerative grade, as well as a more linear behaviour overall (Iatridis *et al.*, 1998). In torsional shear, anulus tissue also displays a trend for increasing stiffness, as well as increased energy dissipation, with increasing degeneration (Iatridis *et al.*, 1999).

The hydraulic permeability of the anulus in the radial direction decreases with degeneration, while circumferential and axial permeabilities increase, resulting in overall reduced anisotropy with respect to this property (Gu *et al.*, 1999).

1.2.1.5.4 In Vitro Assessment of Disc Condition

A number of schemes exist by which the degenerative condition of discs can be assessed in vitro. They generally consist of ranking discs at four or five different levels, with grade one discs showing no signs of degeneration and grades four or five showing the most severe degeneration. The most common grading techniques are morphological and radiological (Wagner *et al.*, 1988; Thompson *et al.*, 1990; Schiebler *et al.*, 1991; Berlemann *et al.*, 1998; Goh *et al.*, 2000; Pfirrmann *et al.*, 2001). Figure 1.10 illustrates the five stages of degeneration as defined by the widely applied scheme of Thompson et al. (1990). Disc grading is discussed in further detail in Chapter 2.

NOTE: This figure is included on page 36 of the print copy of the thesis held in the University of Adelaide Library.

Figure 1.10. Comparison of disc degenerative grades (anterior-posterior sagittal sections) (adapted from (Thompson *et al.*, 1990)).

1.2.2 Elastic Fibres

1.2.2.1 Biochemistry and Distribution in the Anulus Fibrosus

Mature elastic fibres consist of a core of the protein elastin, which is integrated within a scaffold of microfibrillar glycoproteins (Kielty *et al.*, 2002; Kielty, 2006). Originally considered amorphous, the elastin core has more recently been shown to be comprised of laterally packed, thin-beaded filaments; the microfibrils form loosely packed parallel bundles (Kielty *et al.*, 2002). Molecular constituents of elastic fibres can be divided into three categories: those of the elastic fibre core; those co-localising with micofibrils; and those associated with the core-microfibril interface (Kielty *et al.*, 2002). In the core, the mature, insoluble elastin polymer comprises multiple tropoelastin molecules bound covalently by bi-, tri- or tetra-functional crosslinks, including lysinonorleucine, desmosine and isodesmosine (Debelle and Tamburro, 1999). The principal structural molecules of elastic microfibrils are the fibrillins 1 and 2, and to a lesser extent, microfibril associated glycoproteins (MAGPs). Molecules associated with the elastin-microfibril interface include LTBP-2, fibulin-2, emilin-1, and the proteoglycans versican and decorin (Kielty, 2006). With respect to assembly, a scaffold of fibrillin-rich microfibrils is initially laid down in a complex multistep process about which there is still limited understanding, but which is considered to be similar to that which occurs for other extracellular matrix proteins such as collagens and proteoglycans (Kielty *et al.*, 2002). Newly-secreted tropoelastin molecules are then deposited onto the scaffold where they crosslink to form mature elastin (Kielty *et al.*, 2002). The elastic fibre assembly process is illustrated schematically in Figure 1.11.

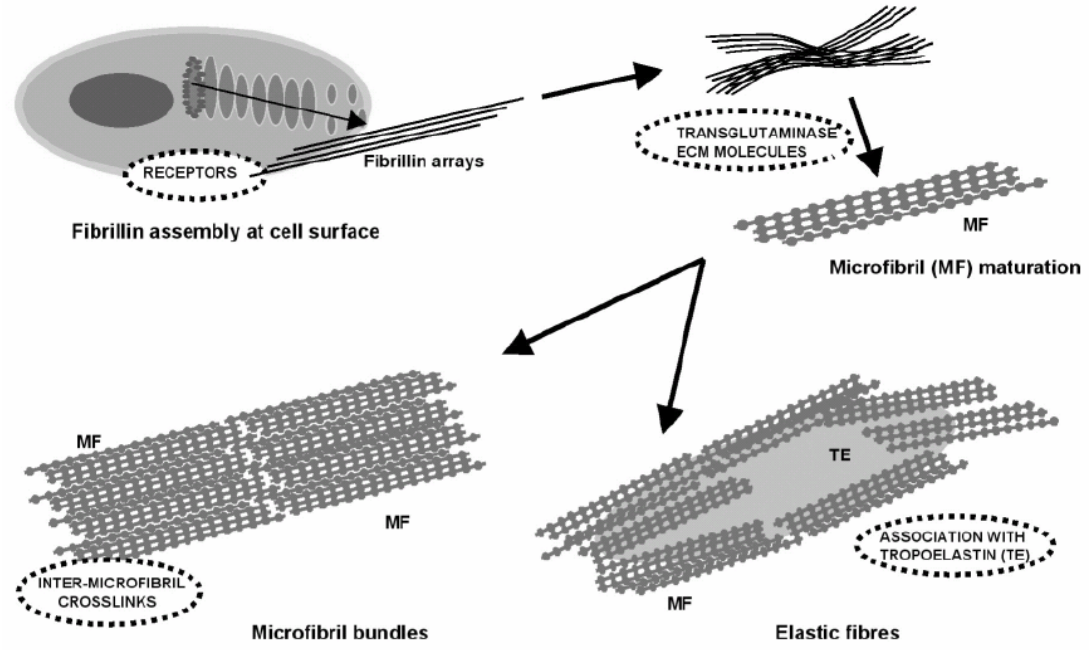


Figure 1.11. The elastic fibre assembly process, illustrated schematically, from microfibril (MF) deposition to subsequent association with tropoelastin (TE) to form the mature fibre (adapted from (Kielty *et al.*, 2002)).

Several proteoglycans, including decorin, byglican and versican are considered to play critical roles in the integration of elastic microfibrils into the surrounding matrix (Kielty *et al.*, 2002). While commonly referred to somewhat generically as either ‘elastic fibres’ or ‘elastin fibres’, specific terminologies exist to describe those with differing ultrastructures and biochemical compositions. These include: mature elastic fibres; *elaunin* fibres, which have a reduced elastin component relative to the microfibrillar component; and *oxytalan* fibres, which have no elastin component and are thus composed entirely of microfibrils (Montes, 1996). As well as existing as fully developed fibres in their own right, during development, elaunin and oxytalan fibres may appear as progenitors of mature elastic fibres (Montes, 1996). Henceforth, use of the term ‘elastic fibres’ in this thesis will encompass all three fibre types. Where the term elastin is used, it is to refer specifically to the primary protein constituent of the mature elastic fibre core.

There have been several studies published in which the elastin or elastic fibre content of the disc has been quantitatively assessed. Using gravimetric methods, Mikawa et al. (1986) found the overall elastin content of the human disc to be 1.7 percent of its dry weight, and that there was no significant difference in content between the anulus and the nucleus. In contrast, using similar methods Olczyk (1994) reported a higher elastin content in the anulus (approximately 2 percent) than in the nucleus (approximately 1.5 percent). Johnson et al. (1985) estimated histologically the overall area occupied by elastic fibres in the anulus to be 10.3 percent. Most recently, Cloyd and Elliott (2007) demonstrated biochemically that the non-degenerate disc contains approximately 2% elastin (in dry weight terms) and displays no significant differences in elastin content between the inner anulus, outer anulus and nucleus.

Ultrastructurally, elastic fibres in both the human anulus fibrosus and nucleus pulposus conform to the typical morphology described, consisting of a central core surrounded by microfibrils (Buckwalter *et al.*, 1976). Age related differences in the ultrastructure of these fibres are consistent with those observed in other tissues, with those of young specimens having a less developed central core (Buckwalter *et al.*, 1976; Hickey and Hukins, 1981; Postacchini *et al.*, 1984). These differences, however, appear to be more pronounced in the anulus fibrosus than the nucleus pulposus (Buckwalter *et al.*, 1976).

Early ultrastructural and microstructural studies of the elastic fibres in the disc led to initial speculation that they may play only a minor mechanical role, due to the perceived sparseness and irregularity of their distribution relative to extracellular matrix elements (Johnson *et al.*, 1982; Postacchini *et al.*, 1984; Mikawa *et al.*, 1986). Johnson, et al. (1982) observed that elastic fibres were particularly prevalent in regions of the disc directly associated with adjacent vertebral bodies. This study noted that fibres appeared to be arranged in successive lamellae in the anulus in circular, longitudinal and oblique orientations, and in the vicinity of the transition zone fibres were observed in a three-dimensional mesh pattern, but were concentrated in areas of where the disc interfaced with the end plate or directly with the vertebral body. A close association between location and orientation of elastic fibres and collagen fibres was observed. It was also noted that elastic fibres, together with collagen fibres extended from the disc into the vertebral body at the anulus periphery by way of Sharpey's fibres, in an apparent anchoring role. It was suggested that elastic fibres may contribute to the recovery of disc shape following deformation. It was also

thought they may assist in the expansion of the anular lamellae by permitting relative elastic movement between the collagen fibrils (Johnson *et al.*, 1982).

Subsequent studies revealed elastic fibres exist in a more extensive and organised network. In the first study to apply both histochemical and immunohistochemical techniques Yu et al. (2002) investigated the elastic fibre content and organisation in intervertebral discs of the bovine tail. Elastic fibres were observed throughout all regions of the disc: a highly structured network of radial and vertical fibres were identified in the nucleus; a mesh structure of fibres was observed in the vicinity of the transition zone; fibres within the anulus lamellae were found to be predominantly parallel to the collagen fibre bundles, and appeared densely concentrated at the interfaces between consecutive lamellae. Additionally, a number of radially oriented 'cross-bridges' of elastic fibres were identified intermittently traversing individual lamellae. Considerable differences in the elastic fibre network were also observed between discs of bovine calves and adult animals, suggesting that the nature of the network changes with age. Subsequently, Yu et al. (2005) confirmed these findings for the human disc (Figure 1.12). Most recently, Yu et al. (2007) examined the distribution of both elastin and fibrillin-1 in intervertebral disc specimens from adolescent humans and bovine tails. Fibrillin-containing microfibrils were found to be co-distributed with elastin in all regions of the disc. In the nucleus, microfibrils were observed both in close association with elastin and in isolation.

NOTE: This figure is included on page 42 of the print copy of the thesis held in the University of Adelaide Library.

Figure 1.12. Elastin immunostaining in the inner region of a healthy human annulus fibrosus showing apparent architectural differences in the elastic fibre network between intralamellar (arrows) and interlamellar (*) regions (adapted from (Yu *et al.*, 2005)).

1.2.2.2 Mechanical Properties

Elastin in isolation exhibits high linear elasticity, is highly extensible and has an elastic modulus of approximately 0.5 MPa (Fung, 1981). The mechanical properties of elastin are distinct from those of fibrillin-containing microfibrils, which have an elastic modulus of between 78 MPa and 96 MPa, around two orders of magnitude greater than that of elastin (Sherratt *et al.*, 2003). Mature elastic fibres can therefore be considered composites in which mechanical properties are defined according to the combined responses of the elastin core and its surrounding microfibrillar scaffold (Sherratt *et al.*, 2003).

The mechanical properties of pure elastin are highly dependant on hydration. Elastic fibres require water to exhibit their rubber-like elasticity. Without the exposure to an appropriate swelling agent, elastin behaves as a rigid solid similar to glass (Gosline, 1976). Because of this, elastin is said to undergo a 'glass transition', which is also dependent on temperature (Kakivaya and Hoeve, 1975).

1.2.2.3 Functional Roles in Composite Tissues

While qualitative microstructural and ultrastructural descriptions of elastic fibre distribution in the anulus have provided an initial framework allowing researchers to hypothesize as to their possible contribution to the mechanical behaviour of the anulus fibrosus, there is currently no direct experimental evidence regarding the nature and magnitude of that contribution. The mechanical role of elastic fibres has however been experimentally described for a number of other dynamic biological tissues, including artery, lung, skin, heart valve and tendon (Armeniades *et al.*, 1973; Karlinsky *et al.*, 1976; Missirlis, 1977; Oakes and Bialkower, 1977; Oxlund *et al.*,

1988; Yuan *et al.*, 2000; Lee *et al.*, 2001). While the mechanical function of each of these tissues is naturally distinct from each other and the anulus fibrosus , a review of the results of these studies can none-the-less be used to further inform the devolopment of hypotheses regarding their possible functional roles in the anulus.

In skin, for example, elastin comprises approximately one percent of the extracellular matrix in terms of dry weight. Elastic fibres form a scattered, delicate network between the collagen fibres. In-vitro studies have found that these elastic fibres influence the mechanical properties of skin at small stress values and small deformations, but do not contribute to the overall strength of the tissue (Oxlund *et al.*, 1988).

The elastin content of the human aorta peaks at approximately 50 percent with maturity (Scarselli, 1961). Elastic fibres form dense concentric laminae between the intimal and medial, and between the medial and advential layers of the artery and, additionally, within the medial layer, co-distribute with collagen fibres and smooth muscle cells (Kielty, 2006). In circumferentially oriented specimens from the aortic wall, degradation of elastin has been observed to cause a large decrease in toe region modulus, a decrease in extensibility, but little change in higher strain properties (Armeniades *et al.*, 1973; Missirlis, 1977). In longitudinally oriented aortic specimens, differences have been observed in the mechanical contribution of elastic fibres between human and bovine specimens: in human specimens, removal of elastin resulted in a large decrease in initial toe-region modulus, with minimal change in ultimate modulus (similar to circumferential specimens); in contrast, in bovine specimens, elastin degradation resulted in both a reduced initial modulus and a loss of structural integrity at higher strains. These differences have been attributed to the

additional structural complexity present in bovine specimens (Armeniades *et al.*, 1973; Missirlis, 1977).

In the aortic valve, where elastin constitutes around 13 percent of the dry tissue weight, it has been theorised that elastic fibres act as a 'house keeper', by restoring the rest state mobile collagen fibres within the matrix following large deformations (Vesely, 1998). Elastic elements are arranged in a complex network of sheets, tubes and fibres; the nature and magnitude of their tissue-level mechanical contributions has been demonstrated to be unique in each layer of the valve and with varying orientations (Vesely, 1998). In general, following removal of elastic elements, valves have been observed to undergo passive distension, possibly due to an associated relaxation of the collagen matrix, and exhibit reduced initial modulus under tensile loads (Figure 1.13A) (Missirlis, 1977; Lee *et al.*, 2001). In one case, elastic modulus at high strains was observed to increase following elastin degradation (Lee *et al.*, 2001).

The functional roles of elastic fibres, together with their mechanisms of interaction with co-distributed collagen, have also been studied in the elastic wing tendon of the domestic fowl, a tissue morphologically similar to the ligamentum nuchae (Oakes and Bialkower, 1977). Following selective removal of elastin from the tissue matrix, the initial 'toe region' of the stress-strain response was eliminated, presenting as a large decrease in extensibility; it was observed that the conformational folding of the collagen matrix in the unloaded tissue had relaxed, and histological analyses suggested that this rest state morphology was maintained by elastic fibres. Additionally, a reduction in the tensile strength of the tendons was observed, attributed to possible non-specific action of the enzyme used to degrade elastin on the

tissue collagen. This side-effect has been avoided in most subsquent studies by the inclusion of a specific inhibitor (described further in Chapter 5).

In the healthy, mature human lung, elastin constitutes approximately 30 percent of the dry tissue weight (Chrzanowski *et al.*, 1980). Elastic elements form a complex, three-dimensional fibrous network, interwoven with collagenous elements, and there is evidence of mechanical connections between the two (Toshima *et al.*, 2004). In a guinea pig model, the effect of enzymatically removing elastin on the quasi-static mechanical properties of lung parenchymal strips was to cause a large reduction in initial modulus and an increase in extensibility (Figure 1.13B) (Yuan *et al.*, 2000). In a hamster model, similar enzymatic degradation of elastin in intact lungs resulted in a significant increase in tissue compliance but only at low and medium inflation volumes, suggesting that at high inflation volumes, mechanical behaviour is largely determined by collagenous elements (Karlinsky *et al.*, 1976). These apparently contrasting results compared to those observed at the tissue level suggest that the application of uniaxial strains may lead to a different response than that resulting from a uniform expansion of the entire organ (Yuan *et al.*, 2000).

Comparing each of these tissues, it is apparent that the nature and magnitude of the contribution made by elastic fibres to quasi-static mechanical properties varies considerable with tissue type. Figure 1.13A and Figure 1.13B illustrate this by comparing the contrasting changes in the quasistatic responses for aortic valve tissue and lung tissue respectively following selective degradation of elastin. These differences may be attributable to a number factors, including relative orientations of elastic and collagenous constituents with respect to the direction of the applied load, the ability of fibrous elements to straighten and reorient within the tissue towards the

loading direction, the existence and nature of physical connections between co-distributed elastic and collagenous elements, and the overall relative amounts of each constituent present.

NOTE: This figure is included on page 48 of the print copy of the thesis held in the University of Adelaide Library.

Figure 1.13 The effect of elastase treatment on the quasi-static mechanical properties of A. aortic valve tissue strips (Lee *et al.*, 2001) and B. lung tissue strips (Yuan *et al.*, 2000). A comparison of the elastase treated responses for these architecturally distinct tissues reveals the extent to which tissue structure determines the nature of the contribution made by elastic fibres to the overall mechanical properties.

1.2.2.4 Roles in Disease and Aging

Elastic fibre loss and damage are major contributing factors in the degradation of many tissues. Typically, pathogenesis begins with a decrease in the proportion of microfibrils to elastin, followed by degradation of the elastin core (Kielty, 2006).

Three of the most common degenerative conditions affecting dynamic tissues resulting from elastic fibre degradation are: vascular aneurysm formation, a remodeling cascade initiated by a local elastin defect in the artery wall and occasionally leading to rupture; pulmonary emphysema, in which elastic fibre degradation resulting from a genetic disorder (early onset) or prolonged exposure to toxins (such as from smoking) impedes normal lung mechanical function; and photo-aging of skin, in which elastic fibre damage resulting from chronic exposure to solar radiation impedes normal elasticity and resilience (Watson *et al.*, 1999; Humphrey and Canham, 2000; Kielty, 2006). Hereditory disorders such as Marfan's syndrome and Beal's syndrome directly affect fibrillin-containing microfibrils, leading to severe vascular disease and physical deformity (Kielty, 2006).

In the intervertebral disc, there is conflicting evidence as to whether elastic fibres, as a percentage of the total tissue, increase or decrease with aging and degeneration. Using gravimetric techniques alone, an early study found no apparent change in total elastin content of the intervertebral disc with age (Mikawa *et al.*, 1986). In a subsequent study however, using both biochemical and gravimetric techniques, it was found that the elastin content as a percentage of total dry tissue weight increased steadily in both the anulus and the nucleus until reaching a peak at approximately 40 years, then decreasing progressively until death (Olczyk, 1994). The peak elastin content of the anulus (in terms of dry weight) was found to be approximately two percent, and the

peak elastin content of the nucleus was found to be slightly less, at approximately 1.6 percent. In addition, it was found that the elastin to collagen ratio decreased steadily from birth until death, and that the elastin to glycosaminoglycan ratio increased steadily until approximately the age of 40 before plateauing. In contrast to the findings of Mikawa et al. (1986), it was found that there were significant differences in elastin content between the anulus and nucleus, and that the changes in content with age occurred at different rates. Recently, degeneration related variations in the elastin content of human discs were described (Cloyd and Elliott, 2007). In terms of dry weight, the mean elastin content, measured using a commercial dye-binding assay, of non-degenerate discs was found to be approximately two percent. Elastin content was found to be positively correlated with degeneration, with the highest elastin content of 9.3 percent occuring in the inner anulus of degenerate specimens. Additionally, degenerate specimens exhibited significant differences in elastin content between the inner anulus, and the outer anulus and the nucleus.

There is some evidence that elastic fibre network architecture in the disc changes as a result of spine related pathologies. The arrangement of fibres in discs removed from cases exhibiting neuromuscular and idiopathic scoliosis is sparse and disorganised compared with that observed in discs from non-scoliotic cases (Yu *et al.*, 2005). It is unclear however, whether these changes are causal or consequential with respect to the pathology.

Deposition, degradation and remodelling of the anulus fibrosus elastic fibre network is likely mediated by specific serine proteases, matrix matalloproteinases and their respective tissue inhibitors. Elastic fibre molecules are readily degraded by the serine proteases pancreatic and neutrophil (or leukocyte) elastase, as well as several matrix

metalloproteinases including MMP-2, MMP-7 (matrilysin), MMP-9 and MMP-12 (metalloelastase) (Mecham *et al.*, 1997; Ishii and Asuwa, 2000; Kielty, 2006). In the disc, only limited descriptions of the presence and function of these enzymes currently exist. MMP-7 expression by cells of the nucleus and inner anulus has been demonstrated, more so for degenerate discs and those having suffered prolapse than for non-degenerate discs (Le Maitre *et al.*, 2006). MMP-2 has been shown to be present in nucleus material from discs suffering from the early stages of degeneration, and also in the vicinity of nuclear clefts and anular tears in degenerate discs (Weiler *et al.*, 2002; Kozaci *et al.*, 2006). MMP-9 has been found to be expressed only at very low levels (Weiler *et al.*, 2002). As of yet no studies examining the presence of MMP-12 appear in the literature. Serine elastase has been identified in the human disc, and while its activity was shown to be greater in the anulus than the nucleus, its function remains undetermined (Sedowofia *et al.*, 1982).

The lack of detailed histological descriptions of elastic fibre network architecture and heterogeneity, as well as experimental descriptions of elastic fibre mechanical function in the intervertebral disc, makes it difficult to postulate as to what the consequences of degenerative, hereditary or chronological elastic fibre related disorders would be for normal intervertebral disc behaviour, and to develop treatments accordingly.

1.3 Study Objectives

The literature review presented identifies multiple key areas relating to both the structure and function of the human lumbar anulus fibrosus elastic fibre network that have, to date, not been satisfactorily described. Structural descriptions have been qualitative and limited in scope, and quantitative studies of elastic fibre distribution are yet to be undertaken. Understanding of the structural and functional associations between elastic fibres and collagen exists in theory only, and while analytical models predict that the functional contribution of non-collagenous constituents such as elastic fibres to anulus behaviour is significant, no experimental studies have examined the nature and magnitude of this contribution.

The first objective of this thesis was to characterise the structure of the anulus elastic fibre network by performing a quantitative histological analysis of variations in elastic fibre density in the anulus with both radial and circumferential position, and by conducting a multi-planar comparison of patterns of elastic fibre distribution at distinct levels of the collagen structural hierarchy. The second objective was to investigate the nature of structure-function associations between elastic fibres and collagen, and to do so with specific reference to the distinct structural mechanisms which facilitate tensile deformation of the anulus collagen matrix: straightening of collagen planar crimp; and relative reorientation between adjacent collagen fibres within lamellae and between adjacent lamellae. The final objective was to investigate the nature and magnitude of the contribution made by elastic fibres to the quasi-static tensile mechanical response of the anulus at the tissue level, and, additionally, to examine possible dependance of that contribution on circumferential position and degenerative condition.

CHAPTER 2: SPECIMEN RETRIEVAL AND GRADING

2.1 Introduction

A large number of methods currently exist under which lumbar discs can be graded for degenerative condition; in fact, a recent review identified a total of 22 such schemes (Kettler and Wilke, 2006). Grading techniques range from assessment of macroscopic anatomy, to histology, plain radiography, magnetic resonance imaging and discography. Histology was not feasible for this study, as the associated processing would have compromised the viability of the tissue for biomechanical testing. Schemes involving macroscopic assessment of disc anatomical characteristics, either from transverse or sagittal sections, are the most widely applied for in-vitro studies. Of the macroscopic grading schemes in the literature, that of Thompson et al. (1990) is one of the most widely used, in part due to its demonstrated statistical repeatability (Kettler and Wilke, 2006). This scheme was therefore selected for this study, with some minor adaptions incorporated to account for differing methods of disc excision. Additionally, plain radiographic images and bone mineral density scans of complete lumbar spines were used as required to assess the condition of hard tissue elements adjacent to each disc.

2.2 Methods

For the experimental studies described in this thesis, a total of twelve human lumbar spines were obtained following routine autopsies conducted in the mortuary of the Royal Adelaide Hospital. All material was collected with the approval of the Royal Adelaide Hospital Research Ethics Committee (approval number 010513) and informed consent of next of kin. The details for each case are provided in Table 2.1. In all cases, the cause of death was determined to be unrelated to the musculoskeletal system.

Intervertebral disc condition has been shown to correlate highly with age (Battie and Videman, 2006). For this reason, cases outlined in Table 2.1 were selected to incorporate a wide age range considered most likely to deliver a spread of discs encompassing a broad range of conditions. Following retrieval, spines were thawed at room temperature, x-rayed (Faxitron; Hewlett Packard, Palo Alto, CA, USA) and subjected to bone mineral density scans (QDR-1000; Hologic, Bedford, MA, USA). Using x-rays, adjacent vertebral bodies were assessed for evidence of osteophytes and the condition of vertebral body margins was noted. Spines were then wrapped in saline-moistened gauze, double-sealed in plastic bags, and frozen at -80°C until required.

Prior to disc excision, spines were thawed overnight at 4°C. Ligament and musculature surrounding the disc was flensed, and the presence of any rim lesions was noted. Transverse cuts were then made superiorly and inferiorly to each disc adjacent to the vertebral bodies and endplates using a scalpel, enabling whole discs to be removed. Disc dimensions, including anterior height, and lateral and anterior-

posterior widths were measured using digital calipers. Discs were then hemi-sected anteriorly-posteriorly, and the interior sagittal faces photographed.

The condition of the anulus and nucleus were then assessed according to the features in listed Table 2.2 using the worksheet in Appendix 1, and a grade ranging from 1 to 4 was assigned, where a grade of 4 corresponded to the most degenerate. The modified grading scheme only permitted limited assessment of end-plate condition. All grading steps were undertaken twice by independent assessors. Any conflicting results were resolved through consultation with a third assessor.

Following grading, hemi-discs were individually wrapped in phosphate buffered saline-moistened gauze, sealed in plastic and frozen at -30°C until required for histological, biomechanical or biochemical analyses.

Age	Sex
16	Male
28	Male
40	Female
53	Male
54	Male
57	Male
60	Female
66	Male
76	Female
80	Male
82	Male
87	Female

Table 2.1. Age and sex information for cadaveric lumbar spines.

NOTE: This table is included on page 58 of the print copy of the thesis held in the University of Adelaide Library.

Table 2.2. Disc grading criteria, adapted from (Thompson *et al.*, 1990).

2.3 Results

Example x-ray images are provided in Figure 2.1 and Figure 2.2. Figure 2.1 shows the lumbar spine from the sixteen year old male, with no visible signs of degeneration. Figure 2.2 in contrast, shows the lumbar spine from the 82 year old male, with large osteophytes proximal to the L1-L2 and L3-L4 intervertebral discs. Additionally, the vertebral body margins are pointed, and the L2 vertebral body appears to have suffered a partial crush fracture. Figure 2.3A and Figure 2.3B compare the interior sagital surfaces of non-degenerate and degenerate discs respectively.

Specific details of intervertebral discs used in experimental studies, including degenerative grades, are provided in each relevant chapter.

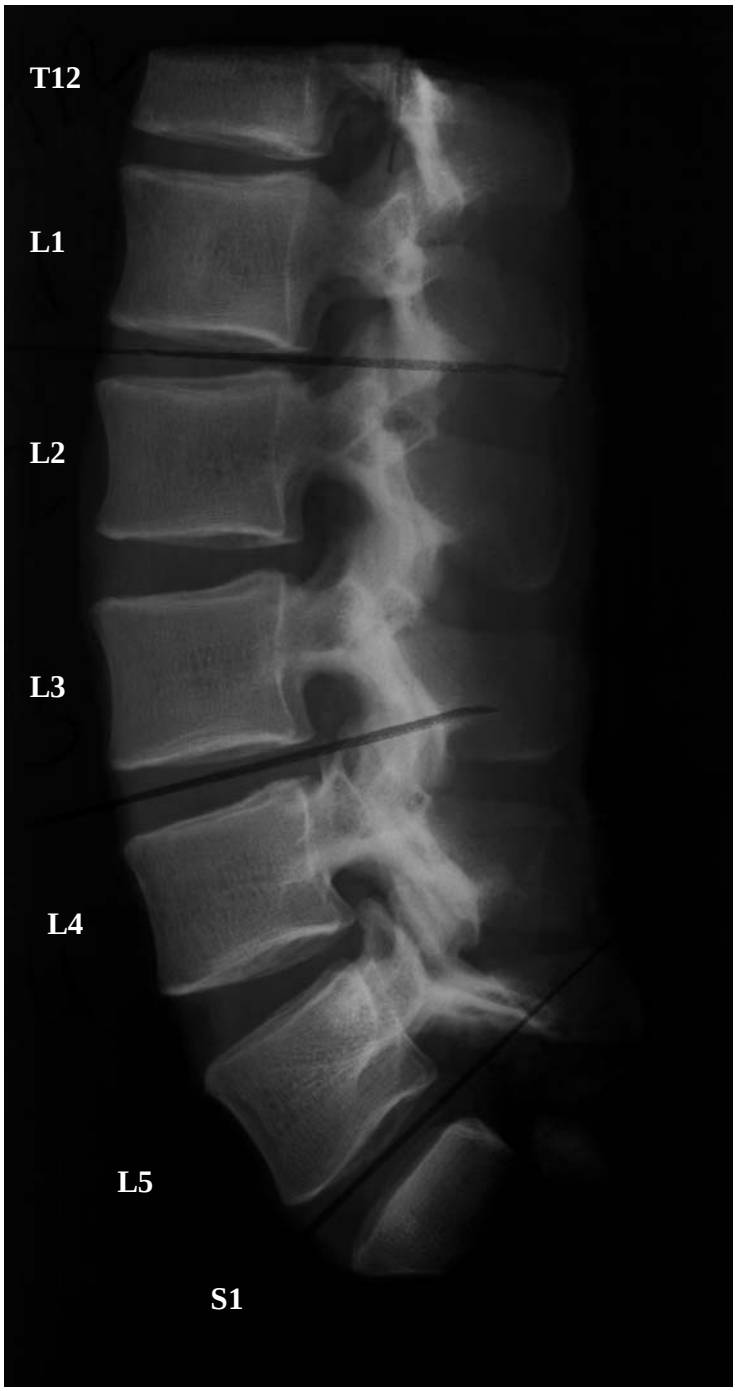


Figure 2.1. X-ray image of the 16 year old lumbar spine. Note the excellent disc height, vertebral body shape and consistent trabecular architecture and volume.

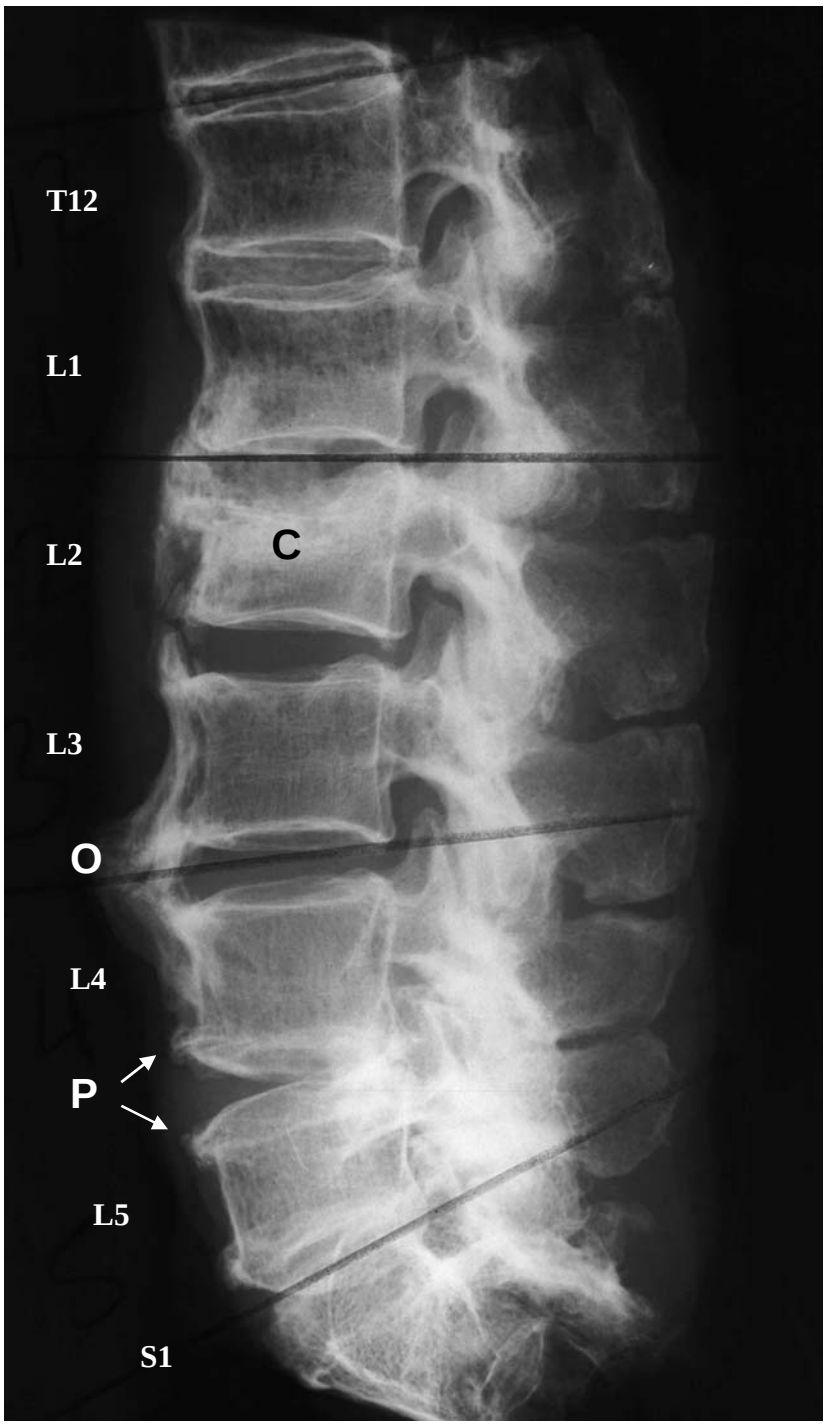


Figure 2.2. X-ray image of the 82 year old lumbar spine. Note the presence of osteophytes (O), pointed vertebral body margins (P), a crush fracture (C) and inconsistent trabecular bone volume between vertebral bodies.

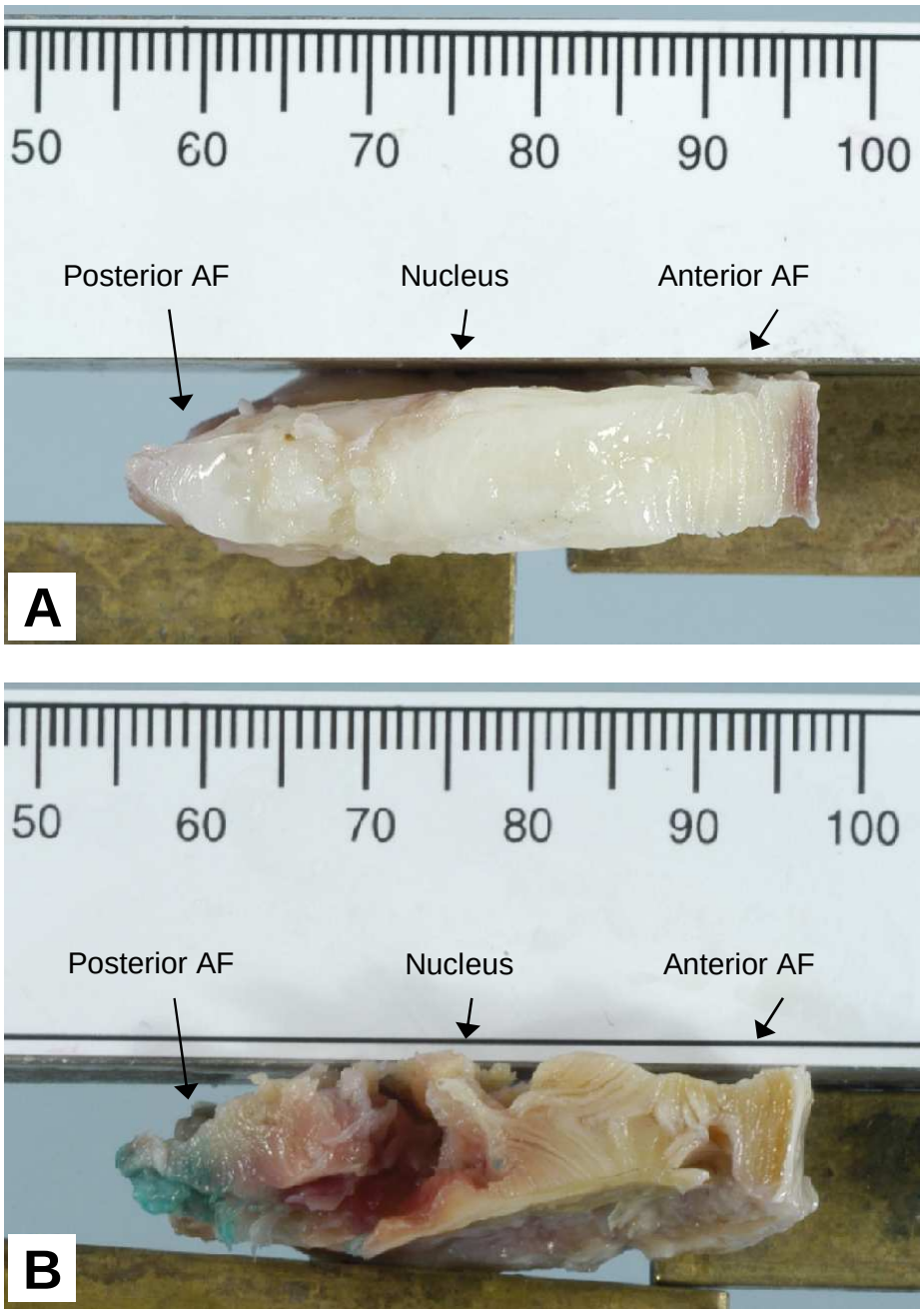


Figure 2.3. Comparison of healthy and degenerate intervertebral discs (mid-sagittal cut). A. Grade 1 L1-L2, 40 year old. B. Grade 4 L1-L2, 87 year old. AF = anulus fibrosus.

CHAPTER 3: STRUCTURE OF THE ELASTIC FIBRE NETWORK

3.1 Introduction

The distribution of elastic fibres in the anulus fibrosus has been examined in a number of histological studies, both at the microstructural and ultrastructural levels (Buckwalter *et al.*, 1976; Hickey and Hukins, 1981; Johnson *et al.*, 1982; Johnson *et al.*, 1985; Yu *et al.*, 2002; Yu *et al.*, 2005; Akhtar *et al.*, 2005a; Akhtar *et al.*, 2005b; Yu *et al.*, 2007). These studies, however have been largely qualitative and limited in scope. Greater understanding of both the arrangement of elastic fibres in the anulus and their relative densities with distance from the periphery and circumferential position is required to provide new insights into their functional roles in healthy discs, including potential contributions to mechanical heterogeneity and anisotropy, as well as their roles in the structural changes associated with degenerative disc disease.

3.2 Scope

Following a statement of objectives and hypotheses, this chapter begins with a review of the literature in which potential experimental techniques are evaluated, followed by methods, results and discussion.

3.3 Objectives and Hypotheses

Objectives in this investigation were to perform a quantitative histological analysis of regional variations in elastic fibre density in the anulus, and to conduct a multi-planar comparison of patterns of elastic fibre distribution in the intralamellar and interlamellar zones.

The following null hypotheses were proposed:

- The density of elastic fibres in the anulus fibrosus of the human lumbar intervertebral disc does not vary with radial position.

- The density of elastic fibres in the anulus fibrosus of the human lumbar intervertebral disc does not vary with circumferential position.

- The arrangement of elastic fibres in the anulus fibrosus of the human lumbar disc does not vary between intralamellar and interlamellar regions.

3.4 Review of Techniques

Four of the most widely applied histochemical staining methods for the demonstration of elastic fibres in connective tissues are orcein, Verhoeff's, aldehyde-fuchsin and resorcin-fuchsin (Sheehan and Hrapchak, 1973; Carson, 1990; Kiernan, 1990; Bancroft *et al.*, 1994). Of these stains, both orcein and Verhoeff's have been successfully used to study intervertebral disc elastic fibres (Johnson *et al.*, 1982; Johnson *et al.*, 1984; Johnson *et al.*, 1985; Yu *et al.*, 2002; Yu *et al.*, 2005).

Orcein stains elastic fibres brown, Verhoeff's blue-black, aldehyde-fuchsin purple and resorcin-fuchsin blue-black. While the principles underlying the binding of the dyes in each of these stains to elastic fibres is poorly understood, they are considered to include, variously, combinations of anionic, covalent and hydrogen bonding and van der Waals forces (Bancroft *et al.*, 1994). Of these techniques, only aldehyde-fuchsin displays sensitivity to the method of tissue fixation, with optimal results achieved using formalin. Aldehyde fuchsin also typically displays greater cross-specificity for other matrix constituents such as cells and granules (Carson, 1990; Bancroft *et al.*, 1994). Resorcin-fuchsin is considered superior to both Verhoeff's and orcein as it stains elastic fibres more intensely. A variant of the resorcin-fuchsin technique (Miller, 1971) combined with a pre-oxidation step using potassium permanganate has been demonstrated to stain elastic fibres at all three stages of development – mature fibres, elaunin fibres and oxytalan fibres (Caldini *et al.*, 1990).

In addition to these methods, elastic fibres have been successfully demonstrated in various tissues using fluorescence and autofluorescence. Visualisation of elastic fibres in haematoxylin and eosin stained sections using either fluorescent light or confocal

laser scanning microscopy has been proposed as a useful tool for the analysis of fibres in archived, routinely stained sections (de Carvalho and Taboga, 1996). Harris' haematoxylin and eosin-phloxine in the ratio 10:1 have been found to produce the best results. When subjected to light with an excitation wavelength of 490 nm, an emission peak occurs at 550 nm. Evaluation of the viability of visualising anulus fibrosus elastic fibres in haematoxylin and eosin stain sections using ordinary fluorescence microscopy, as well as with confocal and muti-photon laser scanning microscopy was conducted experimentally. Seven micron thick transverse sections of intervertebral disc, prepared as described later in this chapter, were stained using recommended published methods (de Carvalho and Taboga, 1996). Briefly, deparaffinised and hydrated sections were stained in Harris' haematoxylin for 4 minutes, differentiated in a solution of 70 percent ethanol and 1 N hydrochloric acid prepared in the ratio 9:1, washed in tap water for ten minutes, then stained in eosin-phloxine prepared as 1 percent mixtures in acidified ethanol in the ration 10:1, dehydrated, cleared and coverslipped. Using a fluorescence microscope attached to a digital imaging station (Leica Microsystems, Wetzlar, Germany), sections were viewed at a range of objective magnifications up to 100 times using the recommended excitation and emmission wavelengths. While some elastic fibres were observed (Figure 3.1), eosin staining of the surrounding collagen matrix and its resulting fluorescence at the same wavelength resulted in their significant obscuration. A similar phenomenon occurred when sections were viewed using confocal or multiphoton laser scanning microscopes. For these reasons, the use of haematoxylin and eosin stained sections for elastic fibre visualisation was not considered viable.

Elastin autofluorescence occurs most prominantly in the spectral range of 405 and 460 nm (blue/green), under excitation wavelengths between 270 and 370 nm. Collagen autofluorescence occurs over a similar spectral range, and as a result differentiation between the two tissue elements is difficult. Multi-photon laser confocal microscopy allows more specific differentiation between elastin and collagen by way of second harmonic generation (Konig *et al.*, 2005). Evaluation of the viability of visualising elastic fibres by way of their autofluorescence in unstained seven micron sections using both fluorescent light and multi-photon microscopy was conducted experimentally. Elastic fibres were successfully observed in unstained, de-paraffinised sections, however their autofluorescence was extremely weak, with finer fibres barely visible at all. As in eosin stained sections, the dense surrounding collagen autofluoresced at a similar wavelength, extensively masking elastic fibres. Additionally, photo-bleaching occurred extremely quickly. For these reasons, visualisation of elastic fibres by way of autofluoescence was not considered viable.

Immunohistochemical techniques are able to selectively demonstrate elastic fibre consituents using specific antibodies for elastin, fibrillins and microfibrillar associated glycoproteins. Both single and double immunostaining is possible, and has been applied successfully in both paraffin sections and cryo-sections from tissues including intervertebral disc and tendon (Ritty *et al.*, 2002; Yu *et al.*, 2007). Immunohistochemical techniques require multiple antibodies to demonstrate all ultrastructural components of elastic fibres (both elastin and microfibrillar), and they are highly sensitive to tissue preparation and fixation methods (Bancroft *et al.*, 1994). Histochemical methods are by comparison simple and robust. Resorcin-fuchsin

preceded by oxidation was selected due to its broad specificity for elastic fibres at all stages of development and greater staining intensity relative to other techniques.

A survey of the literature revealed the most common technique for quantitating elastic fibres in histological sections is one in which the area occupied by elastic fibres relative to the total tissue area in a given field of view is calculated (Johnson *et al.*, 1985; Clement *et al.*, 2006; de Lurdes Pinto *et al.*, 2006). Methods for calculating fibre area vary from automated image processing techniques to manual planimetry. Preliminary studies indicated that the degree of background staining would preclude automated image analysis as a means of area calculation, as it was impossible to threshold images such that elastic fibres became distinct from other surrounding matrix. Due to the large number of frames to be analysed, calculation of areas by manual planimetry was rejected for practical reasons. Instead, a new quantitation method was developed, described in section 3.5.5.

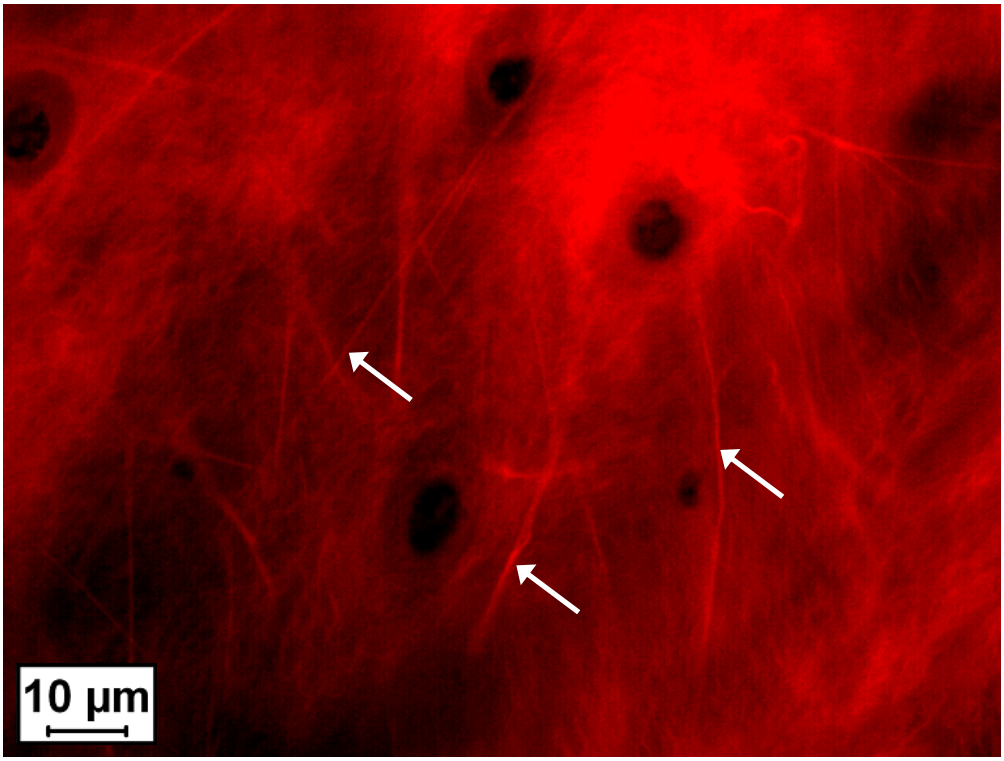


Figure 3.1. Elastic fibres (arrows) in the interlamellar region of a transverse section of anulus fibrosus stained with haematoxylin and eosin, and viewed using fluorescence microscopy at 100 times objective magnification. Elastic fibres are significantly masked by the fluorescence of the surrounding collagen matrix at the same wavelength. Also note the visibility of chondrocyte nuclei (dark circles).

3.5 Methods

3.5.1 Specimen Preparation

Seven intervertebral hemi-discs, excised and graded using the method described in section 2.2, were fixed in 10% buffered formalin for 24 hours, processed using an automated tissue processor (Tissue-Tek VIP5J-F2; Sakura Finetek, Tokyo, Japan) over 48 hours and embedded in paraffin wax. A summary of specimen ages, grades and anterior disc heights is provided in Table 3.1. Also included in this table are bone density T-scores for adjacent vertebral bodies, measured following autopsy retrieval, to enable broad assessment of the influence of bone morphology on results. All intervertebral discs used in this investigation were from the L3-L4 level. This was to negate any possiblity that undocumented variations in elastic fibre density with spine level should confound results. Consecutive sections, 30 μm thick, were cut in the transverse and lamellar planes (illustrated schematically in Figure 3.2) using a sledge microtome (Reichert, Germany) and transferred to a 60°C flotation bath. Between cuts, the tissue block cutting surface was kept moist, as this was found to minimise disruption of the tissue by the microtome blade. Sections were then mounted on 76 by 50 by 1 mm gelatin-coated glass microscope slides and dried overnight at 37°C to ensure sections adhered satifactorily.

Transverse sections were obtained from the approximate mid-axial region of each disc to limit any potential variations in fibre density in the axial direction (i.e. close to the end plates and vertebral bodies) from confounding results. Lamellar plane sections were proximal to the middle anulus of the posterolateral and anterolateral quadrants.

Age	Sex	Disc Height (mm)	Disc Grade	Superior VB* T-Score	Inferior VB T-Score
16	M	12	1	0	0
28	M	9	2	-0.6	-0.8
40	F	13	2	0.3	-0.2
54	M	14	2	-3.6	-3.7
66	M	17	3	-4.7	-5.3
76	F	8	3	-2.1	2
82	M	10	3	0.4	-0.4

Table 3.1. Intervertebral hemi-discs used for examination of elastic fibre network structure, including sex, disc height (anterior), degenerative grade and T-scores for adjacent vertebral bodies. All discs are from the L3-L4 level. *VB = vertebral body

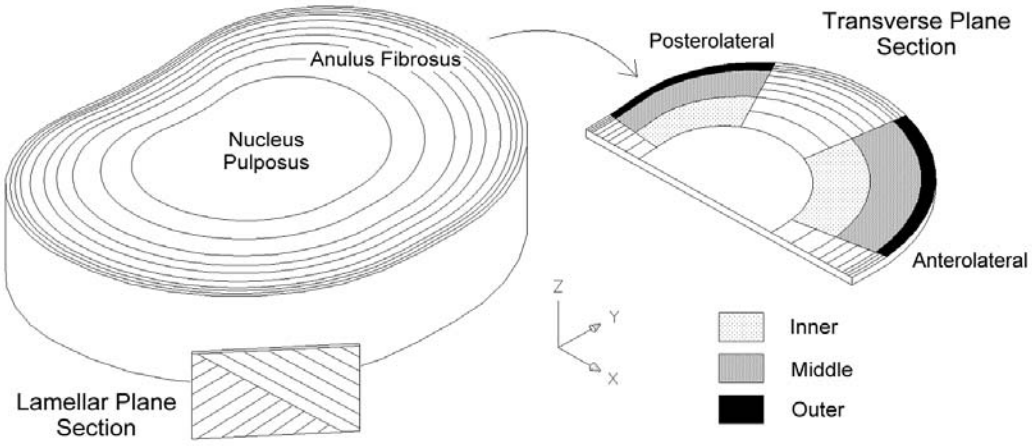


Figure 3.2. Schematic representation of the intervertebral disc illustrating section orientations and sampling zones (radial: inner, middle, outer; circumferential: anterolateral, posterolateral).

3.5.2 Histochemistry

Two histochemical stains were used in this investigation. A van Gieson stain (Curtis' modification) was used to demonstrate general collagenous architecture (Curtis, 1905). A resorcin-fuchsin stain (Miller's modification), preceded by an oxidation step, was used to demonstrate all elastic system fibres, including elaunin and oxytalan fibres (Miller, 1971). Prior to staining with either solution, sections were heated to 60°C for five minutes to melt the paraffin wax, then brought to distilled water through three changes of xylene, two changes of 100 percent ethanol and one change of 70 percent ethanol for five minutes each.

3.5.2.1 Collagen Staining

The van Gieson stain was prepared by combining 90 ml of saturated aqueous picric acid, 10 ml of one percent aqueous ponceau S and 10 ml of glacial acetic acid. Rehydrated sections were flooded with the staining solution for five minutes, then blotted dry using filter paper. They were then rapidly dehydrated in 100 percent ethanol (two changes), cleared in xylene (two changes) and coverslipped with DePeX mounting medium.

3.5.2.2 Elastic Fibre Staining

The resorcin-fuchsin stain was prepared by first dissolving 1 g of Victoria Blue 4R, 1 g of new fuchsin and 1 g of crystal violet in 200 ml of hot water. 4 g of resorcin, 1 g of dextrin and 50 ml of 30 percent aqueous ferric chloride were then added, the mixture was boiled for five minutes, then filtered while hot. The precipitate was redissolve in 200 ml of 95 percent ethanol, and boiled on a hot plate for 15 to 20

minutes. This solution was then filtered and the volume restored to 200 ml with 95 percent ethanol. Finally, 2 ml of concentrated hydrochloric acid was added. Rehydrated sections were oxidised with 0.5 percent aqueous potassium permanganate for ten minutes and washed in deionised water. They were then bleached with 2 percent oxalic acid for five minutes or until colourless, and washed again in deionised water. Sections were equilibrated in 95 percent ethanol for five minutes, then submerged in the resorcin-fuchsin solution for three hours. Each section was then individually washed using 95 percent ethanol from a squeeze bottle to thoroughly remove excess staining solution, then washed in distilled water. Finally, sections were progressively dehydrated in 70 percent, then 100 percent ethanols (two changes), cleared in xylene (two changes) and coverslipped with DePeX mounting medium. Importantly, all sections were stained with the same batch of staining solution. This was considered particularly important with regards to staining consistency in those sections used for quantitation.

Both positive and negative control slides were used to verify that elastic fibres were selectively stained. As positive controls, sections of human artery were stained in parallel with disc sections. As negative controls, a subset of sections was incubated in high purity porcine pancreatic elastase (1 U/ml in 200 mM Tris-HCl, pH 8.6) to selectively remove elastin and stained in parallel (Porter *et al.*, 1977; Caldini *et al.*, 1990).

3.5.3 Microscopy and Imaging

Sections were viewed using an automated microscope (DM6000 B; Leica Microsystems, Wetzlar, Germany) attached to a digital imaging workstation

(Q500MC; Leica Microsystems, Wetzlar, Germany), illustrated in Figure 3.3. The collagen architecture in van Geison stained sections was visualised under cross-polarised light at objective magnifications ranging from 1.5 times to 40 times. In sections stained with resorcin-fuchsin, it was found that elastic fibres were extremely difficult to visualise at magnifications lower than 20 times objective. At 100 times objective magnification (oil immersion) fibres were clearly visible. Additionally, it was found that while fibres were visible under bright field, under phase contrast their clarity was enhanced. Under dark field, fibres appeared bright purple against a dark blue background. Under polarised light, fibres were largely masked by the dense surrounding collagen architecture. Using phase contrast, initially only small fragments of elastic fibres on tissue surface were observed, however, by manually focussing down through the extent of the section, additional detail was revealed. To capture this three-dimensional complexity, a stack of images was taken at between 0.1 and 0.8 micron intervals at an objective magnification of 100 times under phase contrast through the extent of the section thickness (QWin; Leica Microsystems, Wetzlar, Germany). The images in each stack were then merged to produce a single z-projected image (ImageJ; National Institutes of Health USA). These z-series composite images allowed improved visualisation of fibres through the extent of the 30 micron section at high magnifications and were used for the quantitation described in section 3.5.5. Binarising and processing such images (Matlab; Mathworks, Natick, United States) both facilitated the production of three-dimensional reconstructions of elastic fibre organisation, and the overlay of polarised light images with elastic fibres, enabling close examination of elastic fibre and collagen fibre co-distribution. The image processing code can be found in Appendix 2.

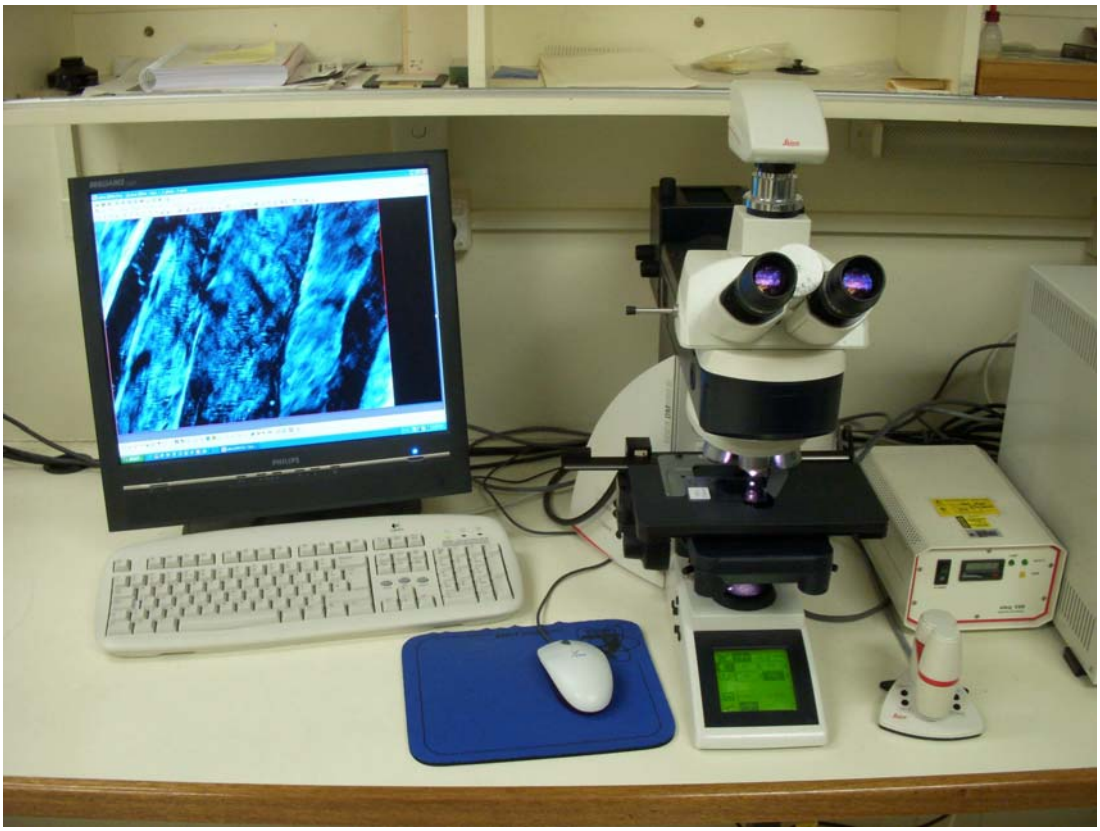


Figure 3.3. Motorised microscope and digitial imaging workstation.

3.5.4 Qualitative Analysis

Patterns of elastic fibre distribution were assessed qualitatively using the composite imaging techniques described. Intra-lamellar distribution patterns were compared between outer, middle and inner lamellae, and between anterolateral and posterolateral quadrants. Additionally, distribution patterns at distinct levels of the collagen matrix hierarchy (i.e. in intralamellar regions and at lamellar and collagen bundle interfaces) were compared. Differentiation between these two regions was initially undertaken using cross-polarised light.

3.5.5 Quantitative Analysis

Quantitation was limited to intralamellar zones of the anulus, as elastic fibre arrangement was observed to be more uni-directional here than in interlamellar zones. Additionally, quantitation was performed exclusively on transverse sections as this planar orientation most easily facilitated the regional analysis.

Using image analysis software, a six by six grid was overlaid on each projected image, (taken at 100 times objective magnification under phase contrast), allowing fibres to be quantified as the mean number intercepted by each horizontal and vertical line of the grid, then normalised as the number of fibres per 100 microns.

To compare regional variations in fibre distribution, the mean results from sets of six fields taken within randomly selected representative collagen lamellae in the outer, middle and inner anulus of the anterolateral and posterolateral quadrants (a total of six regional zones, illustrated in Figure 3.2) were calculated. Distinct radial locations were defined according to established differences in collagen lamella morphology

which occur at increasing distances from the disc periphery (Cassidy *et al.*, 1989; Marchand and Ahmed, 1990).

Statistical analyses were performed using SPSS v.10 (SPSS Inc.; Chicago, United States). To determine the dependence of intralamellar elastic fibre density on circumferential location, paired Student's t-tests were performed comparing overall mean intralamellar elastic fibre density between anterolateral and posterolateral quadrants, as well as at each of the 3 radial locations (outer, middle and inner). Single factor analyses of variance (ANOVAs) were performed to determine if intralamellar elastic fibre density exhibited any significant dependence on radial location (three levels: inner, middle and outer) at each circumferential location (anterolateral and posterolateral). Where ANOVAs showed significant variation, post-hoc pair-wise analysis applying Bonferroni corrections was undertaken. F-tests were performed to compare variances. Significance for all tests was reported at a confidence level of 95%.

3.6 Results

3.6.1 Validation of Staining

Elastic fibre morphology in sections stained with resorcin-fuchsin compared favorably with anulus fibrosus elastic fibres described in the literature and staining intensity was comparable with that observed in positive control sections. No elastic fibres were observed in negative control sections.

3.6.2 Collagenous Architecture

Figure 3.4 shows the collagenous architecture of an entire transverse section from the 28 year old, grade 2, L3-L4 hemi-disc (van Geison stain, polarised light), as a reconstructed image mosaic. Figure 3.5 shows a region of the anterior anulus from the same section at higher magnification. In both these figures, the light and dark bands represent alternating collagen fibre directions in consecutive lamellae. Additionally, in Figure 3.5, the interface between individual collagen fibre bundles in the same lamella can be observed (B), as can a subsplitting of a lamella into multiple bundles across its thickness (S).

Figure 3.6 shows the collagen architecture in a lamellar plane section from the middle anterolateral anulus of the 40 year old, grade 2, L3-L4 disc (van Geison stain, polarised light, 5 times objective magnification), in which collagen bundles, oriented at approximately 30 degrees to the axial plane are clearly illustrated. Figure 3.7 shows a collagen bundle in the same section at higher magnification illustrating the characteristic periodic crimp of the collagen fibres.

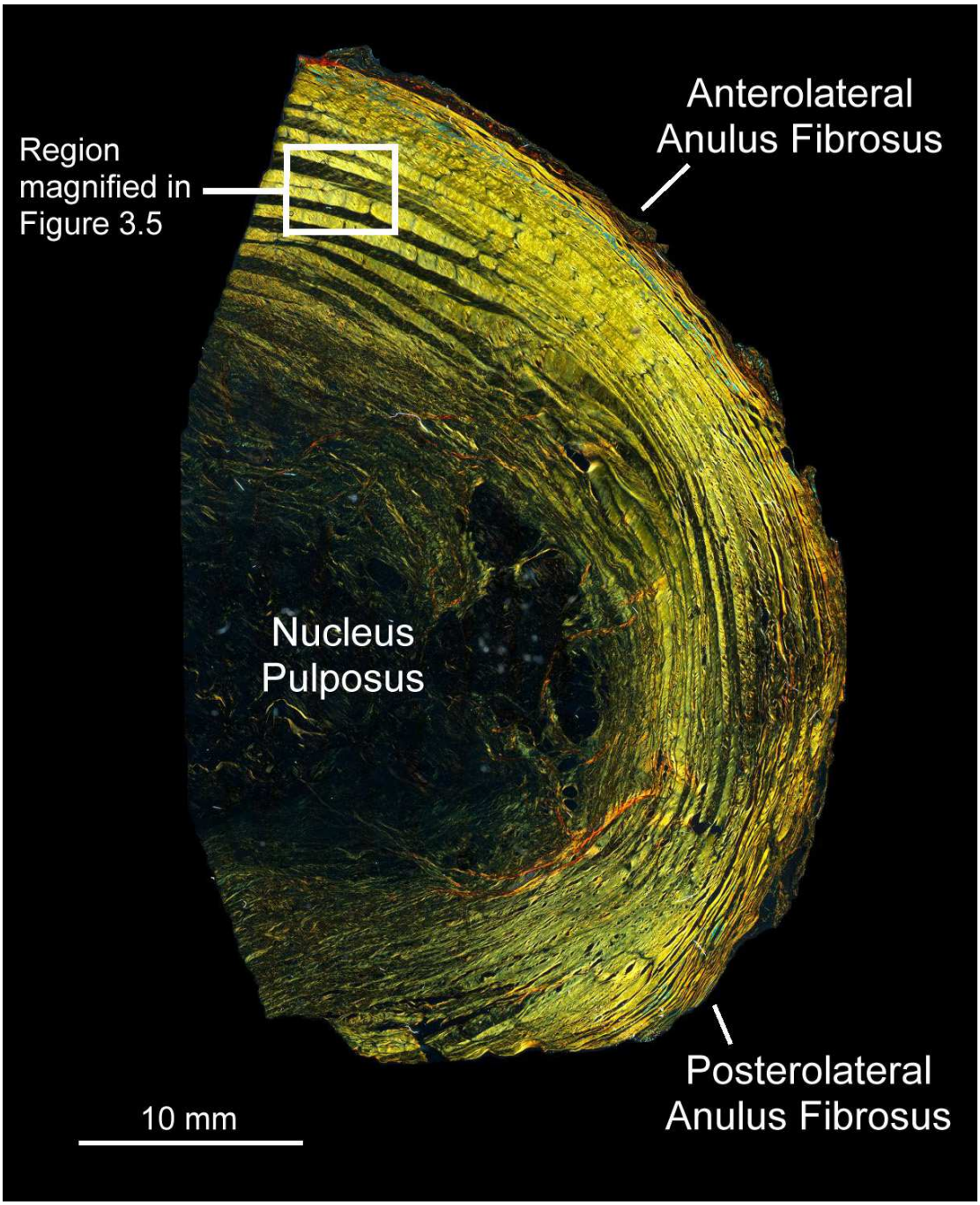


Figure 3.4. Composite mosaic image of an entire hemidisc (28 year old, grade 2, L3-L4, transverse section, van Gieson stain, polarised light). This section was taken directly adjacent to a section used for elastic fibre assessment.

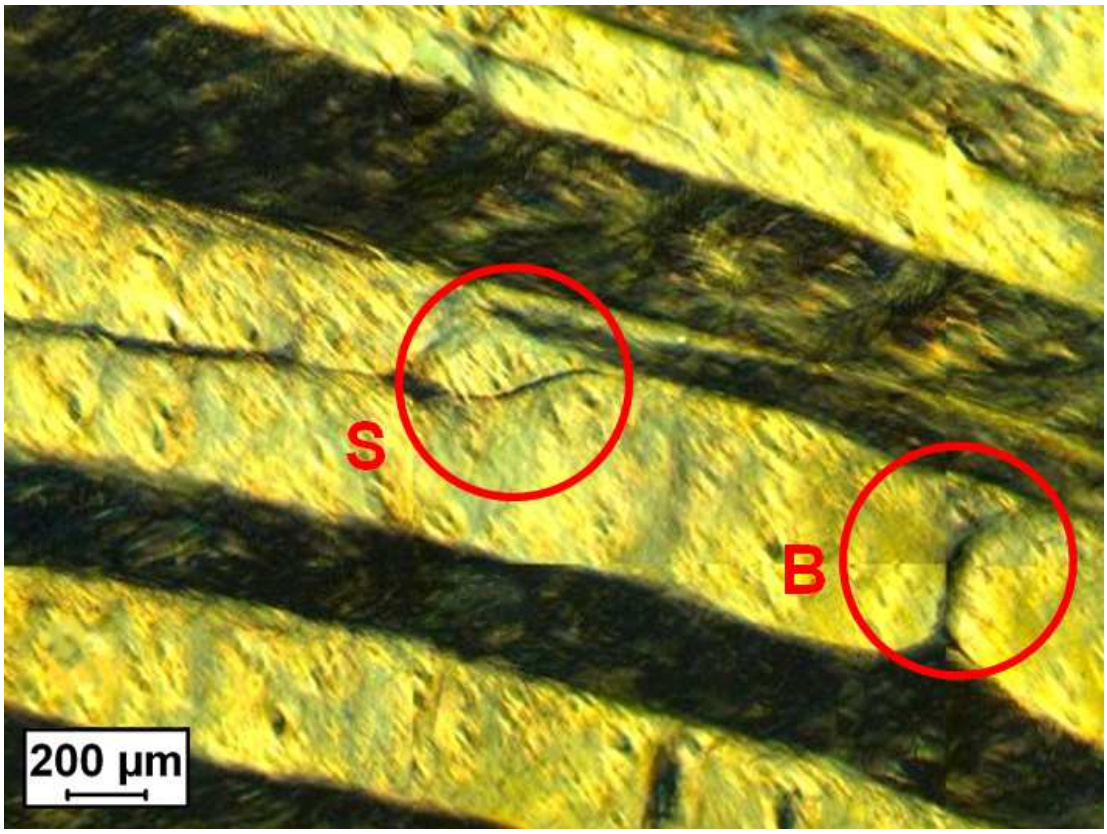


Figure 3.5. Higher magnification view of the region indicated in Figure 3.4. Note the the light and dark bands indicating alternating collagen fibre directions. Also note the presence of subsplitting (S) within a lamellae into multiple collagen bundles across its thickness, and the interface between two adjacent collagen bundles in the same lamella (B). Apparent vertical and horizontal interruptions are artifacts of the mosaic image reconstruction process.

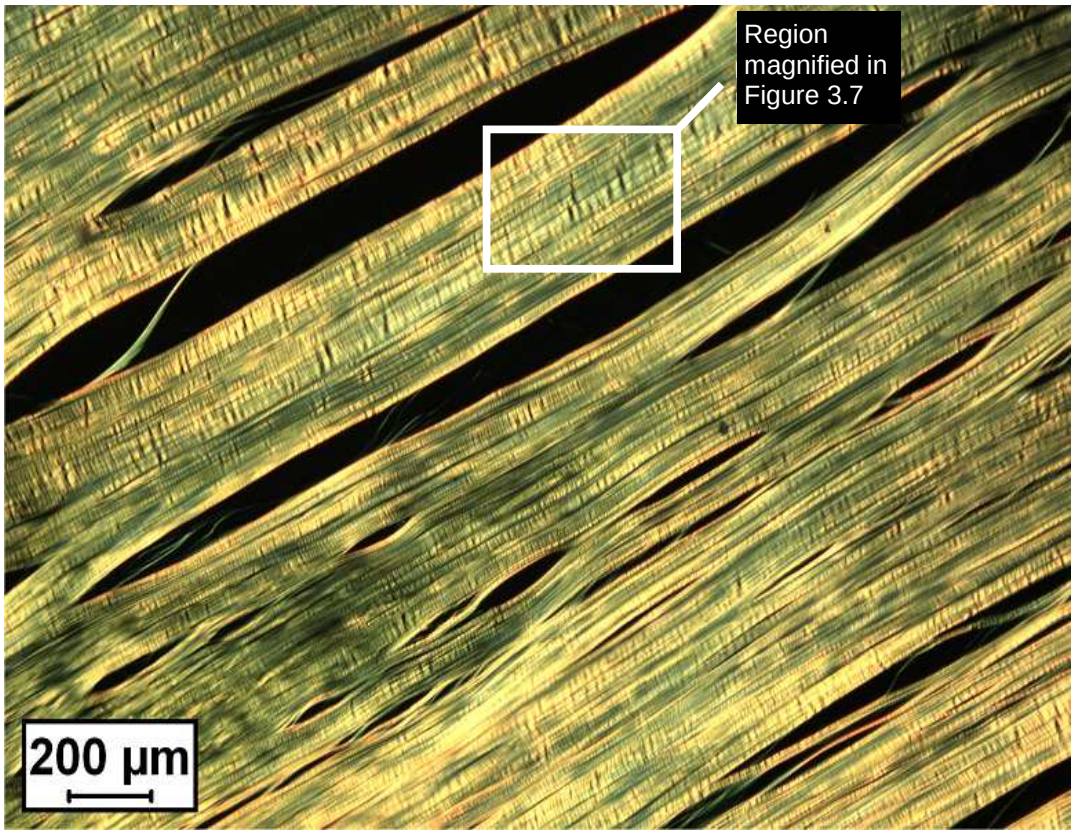


Figure 3.6. A lamellar plane section showing bundles of collagen fibres arranged at approximately 30 degrees to the axial plane of the disc. (40 year old, grade 2, L3-L4, Van Gieson stain, 30µm section, 5x objective magnification, polarised light). This section was taken directly adjacent to a section used for elastic fibre assessment.

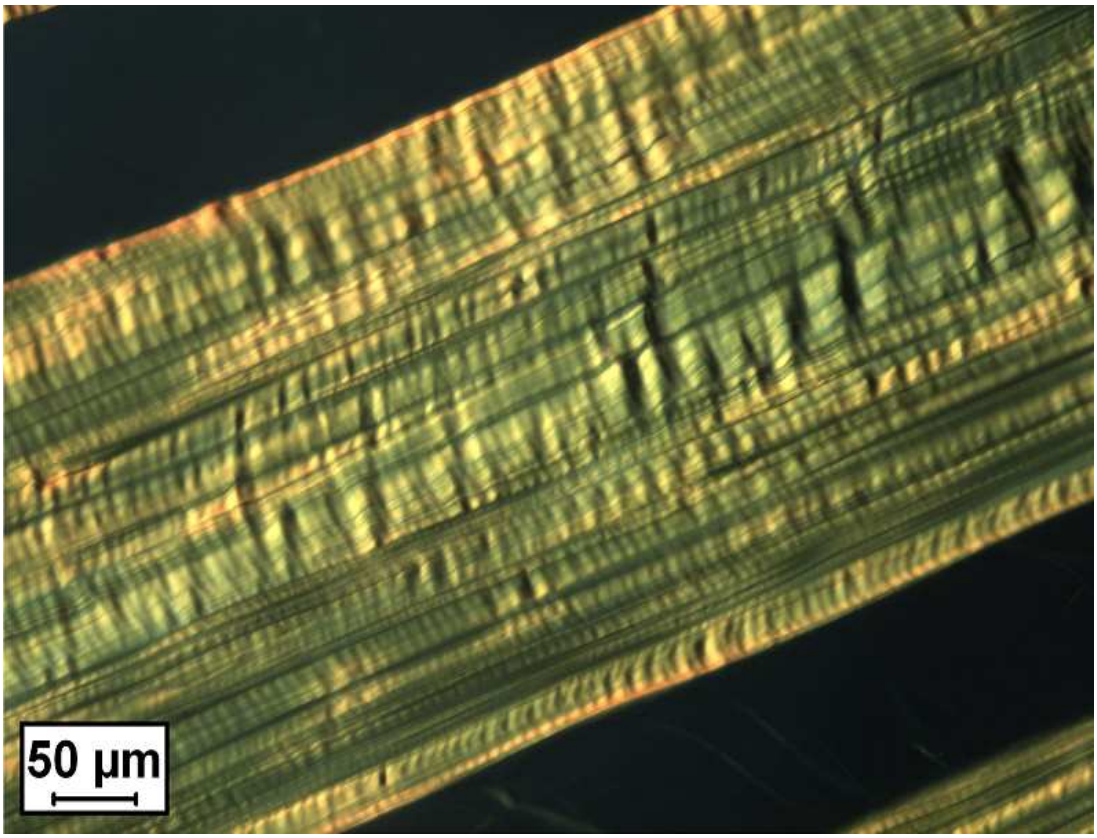


Figure 3.7. Higher magnification view of the region indicated in Figure 3.6. Note the periodic crimp characteristic of the fibrillar collagen.

3.6.3 Elastic Fibre Arrangement in the Intralamellar Zones

In transverse plane sections, intralamellar elastic fibres in the outer regions of the anterolateral anulus appeared straight, tightly packed and with a preferential alignment parallel to the collagen fibres (Figure 3.8). In the outer regions of the posterolateral anulus, elastic fibres, while still straight and tightly packed, formed more random patterns of distribution (Figure 3.9). Figure 3.10 shows a lower magnification, dark field view of the posterolateral anulus which further highlights this additional complexity. In the inner anulus, intralamellar fibres appeared, in general, sparser and more loosely aligned (Figure 3.11). In the lamellar plane, shown under cross-polarised light in Figure 3.12a, the alignment of intralamellar elastic fibres parallel to the direction of the collagen fibres was confirmed (Figure 3.12b, a higher magnification, phase contrast view of the region indicated in Figure 3.12a). Binarising and processing the image in Figure 3.12b enabled elastic fibres to be viewed in isolation (Figure 3.12c), and superimposing this image over the same region viewed under cross-polarised light (Figure 3.12d) allowed closer examination of collagen and elastic fibre co-distribution. Elastic fibres were observed not to be confined to the periphery of the collagen bundles, and in many instances, appeared to conform to the planar crimped pattern of the collagen fibres (Figure 3.12d).

At the interfaces between adjacent collagen bundles within a lamellae (Figure 3.13a), elastic fibres were observed to form networks connecting those bundles. In some cases, these fibres appeared straight, as though under stress (Figure 3.13b), and in other cases, they appeared looser (Figure 3.13c), suggesting a more relaxed state.

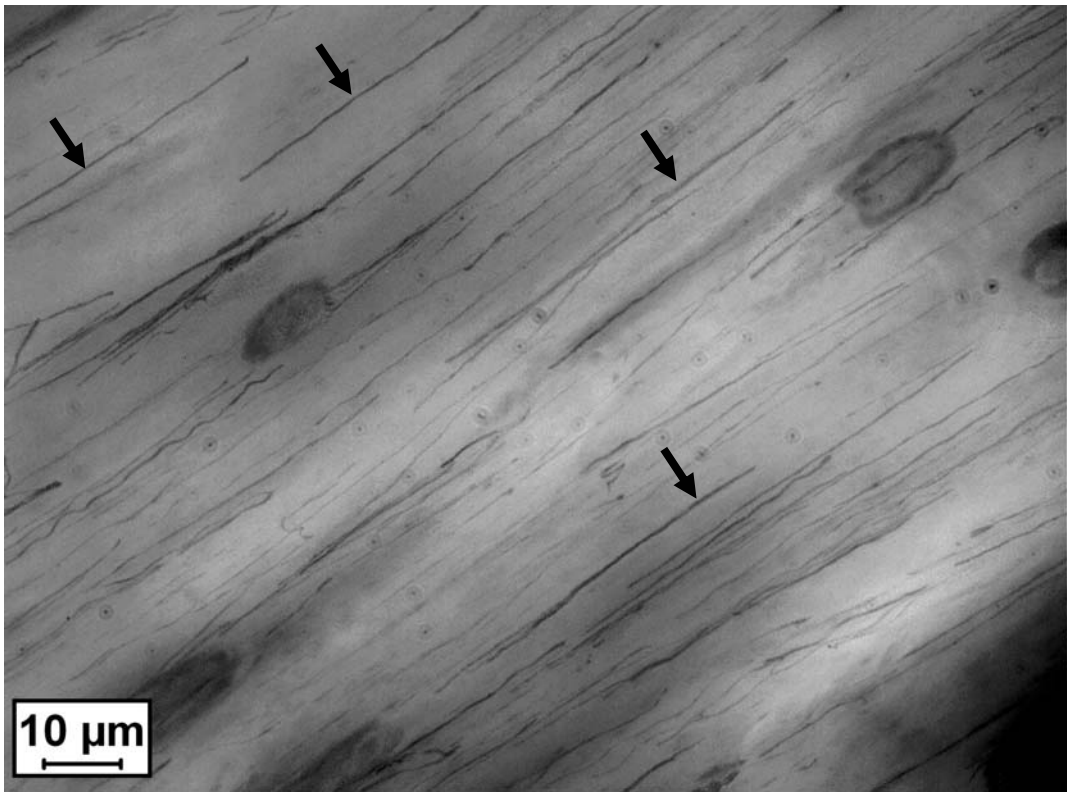


Figure 3.8. Intralamellar elastic fibre arrangement in the outer anterolateral anulus. (Example elastic fibres indicated by arrows; resorcin-fuchsin stain, transverse section, 54 year old, grade 2 specimen, 100 times objective magnification, phase contrast z-projection). Note also the presence of background-stained chondrocyte-like cells, visible as dark ovals.

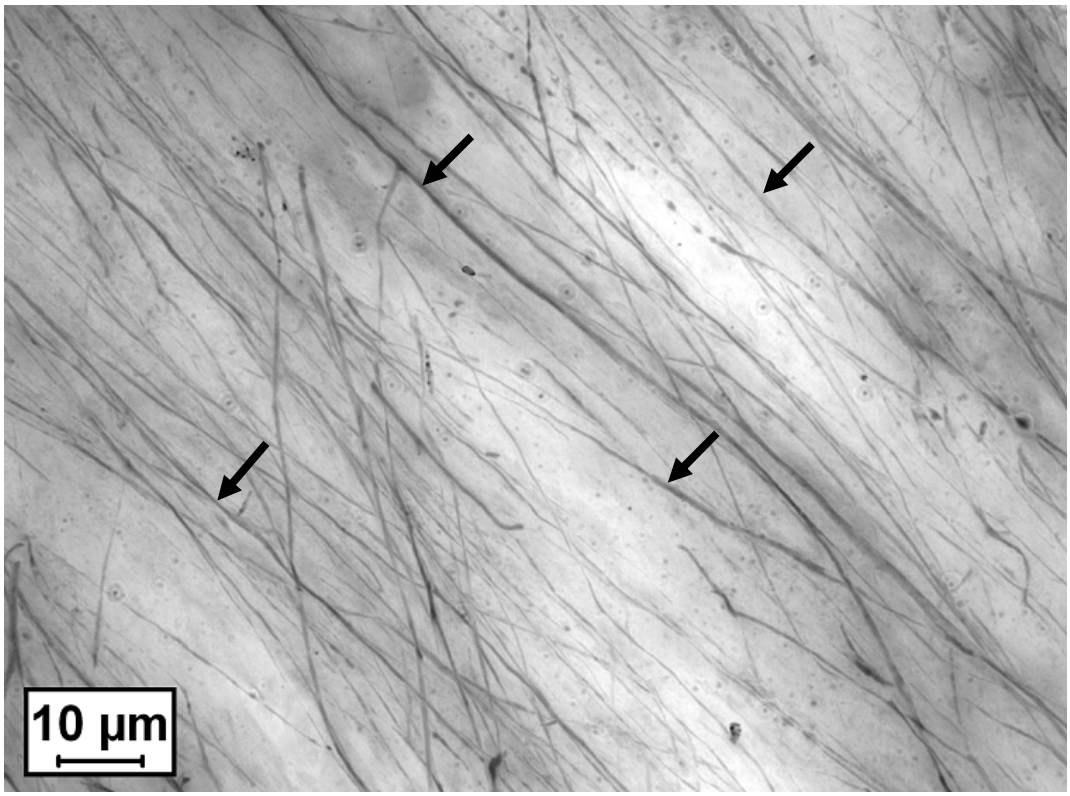


Figure 3.9. Intralamellar elastic fibre arrangement in the outer posterolateral anulus. (Example elastic fibres indicated by arrows; resorcin-fuchsin stain, transverse section, 54 year old, grade 2 specimen, 100 times objective magnification, phase contrast z-projection).

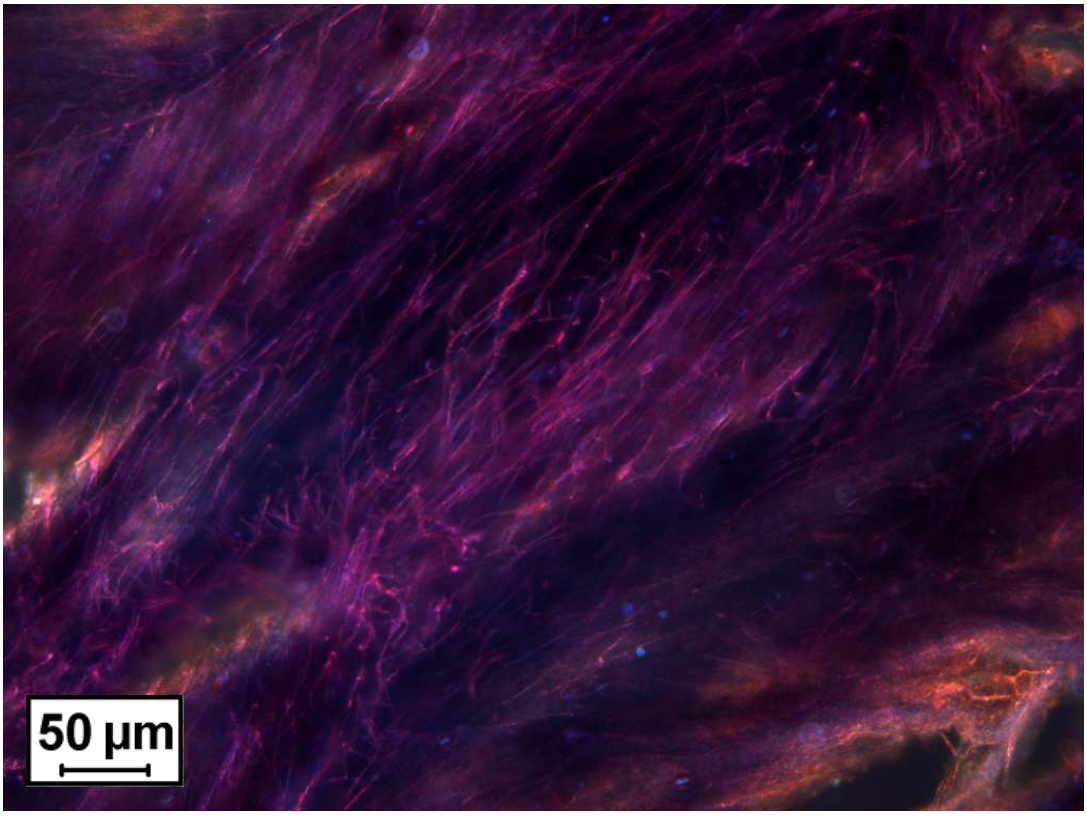


Figure 3.10. Under dark field, elastic fibres appear bright pink/purple against a dark bluish background (image adjusted to improve contrast). This image shows a mass of fibres within the complex lamellar structure of the posterolateral anulus in the 54 year old, grade 2 specimen. (Resorcin fuchsin stain, 30µm section, 20x objective magnification composite z-projected image).

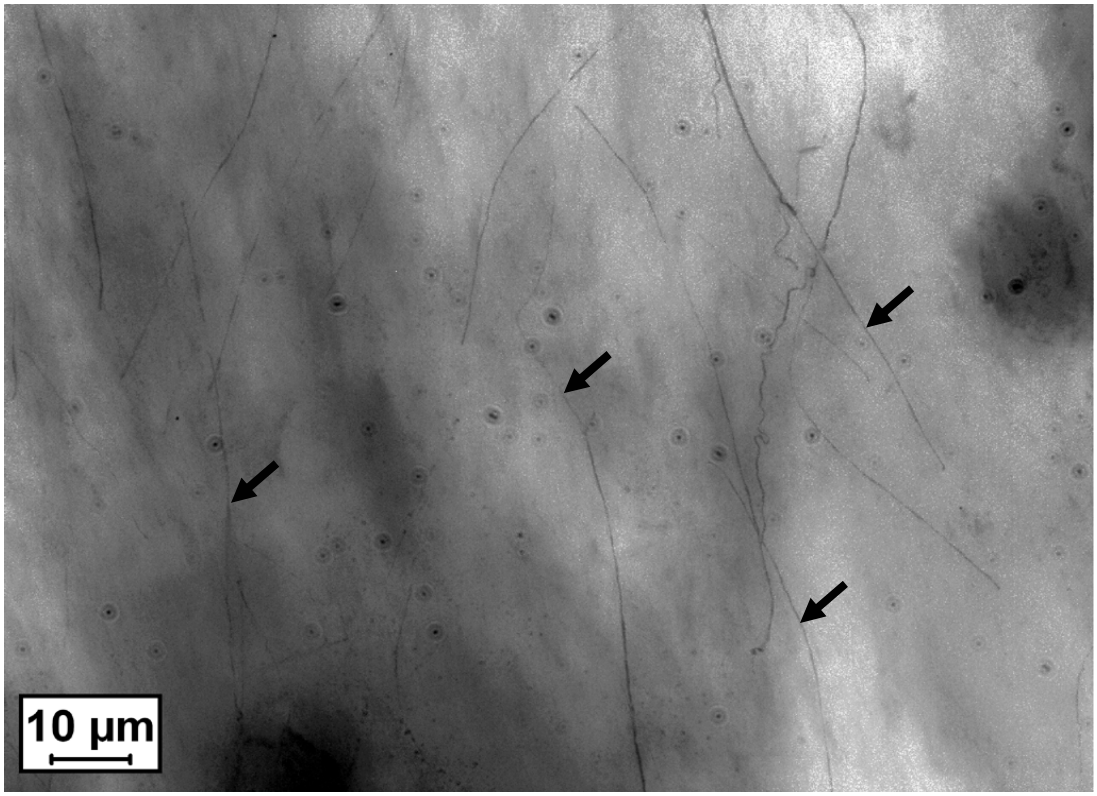


Figure 3.11. Intralamellar elastic fibre arrangement in the inner anulus. (Example elastic fibres indicated by arrows; resorcin-fuchsin stain, transverse section, 28 year old, grade 2 specimen, 100 times objective magnification, phase contrast z-projection).

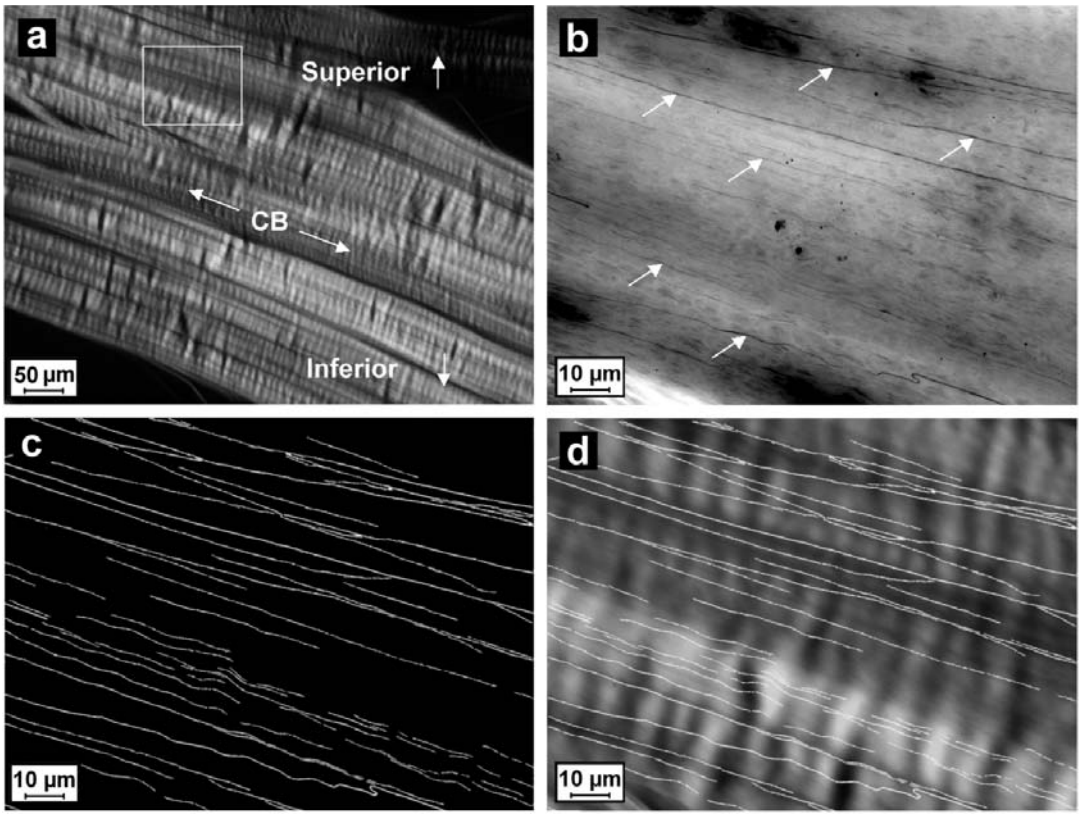


Figure 3.12. Intralamellar elastic fibres and the surrounding matrix architecture of the outer anulus viewed in the lamellar plane. (a) Polarised light image depicting collagen fibre bundles (CB) in the outer anulus of a 40 year old, grade 2 disc angled at approximately 30° to the transverse plane. (b) Higher magnification, phase contrast, z-series composite image in the region of image (a) indicated by the square, showing elastic fibres (examples indicated by arrows) running parallel to the collagen fibril bundles. (c) Binarised reconstruction of (b). (d) Elastic fibres in (c) are superimposed over a high magnification, polarised light view of the same region showing elastic fibre distribution relative to the collagen microarchitecture, including planar crimp.

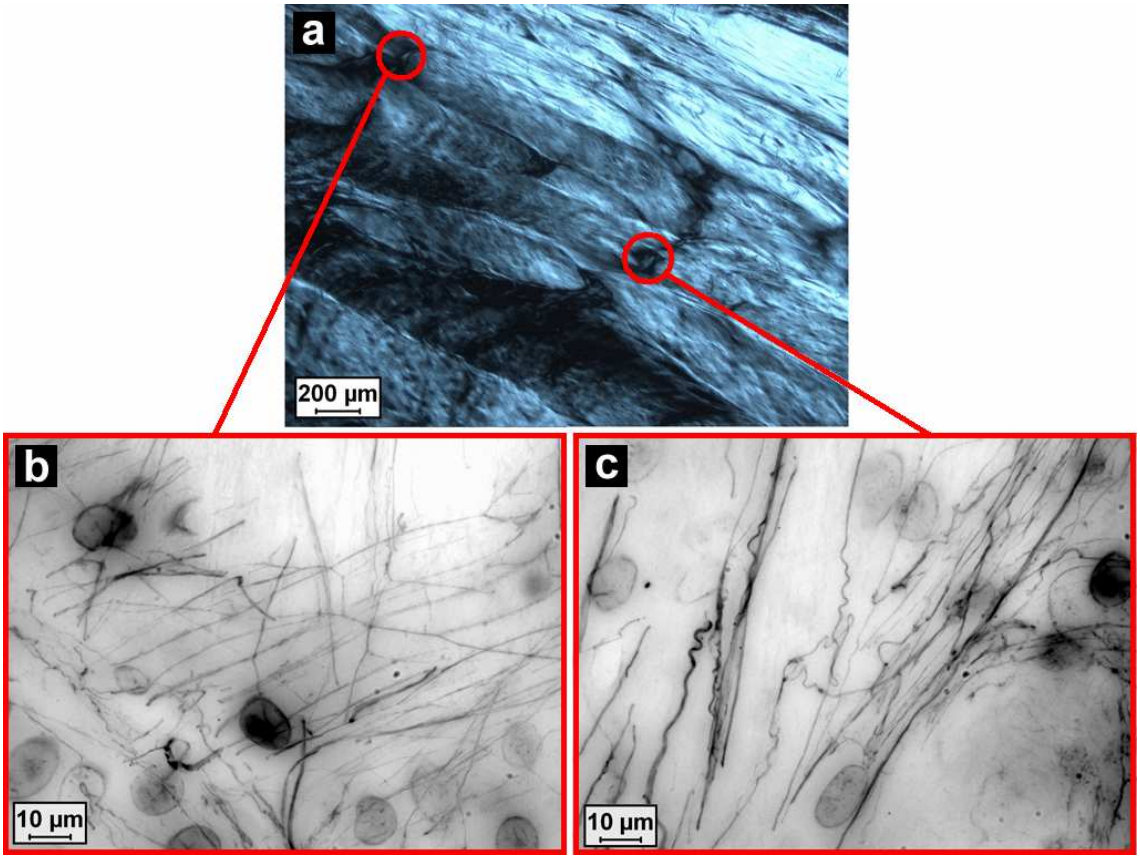


Figure 3.13. Elastic fibre architecture at the intersection of adjacent collagen bundles, viewed in the transverse plane as z series composite images (b and c), contextualised against the surrounding architecture viewed under polarised light (a). In some cases, these fibres appeared straight, as though under stress (b), and in other cases, they appeared looser (c), suggesting a more relaxed state. A large number of non-specifically stained chondrocyte-like cells are also visible. (Resorcin-fuchsin stain; image a viewed under cross-polarised light at 5 times objective magnification; images b and c are bright-field z-projected images viewed at 100 time objective magnification).

3.6.4 Elastic Fibre Arrangement in the Interlamellar Zones

Elastic fibres in interlamellar zones exhibited more complex, multi-directional patterns of distribution compared with those in intralamellar zones. By combining high magnification polarised light and binarised phase contrast images in a manner similar to that described in section 3.6.3, the arrangement of elastic fibres was compared with the micro-architecture of the surrounding collagen matrix. Figure 3.14 and Figure 3.15 depict interlamellar zones in lamellar and transverse plane sections respectively. In both orientations, elastic fibres were observed to form structurally complex meshworks branching out from the collagen bundles to bridge lamellar interfaces. Within these meshworks combinations of both large and very fine fibres were observed, suggesting the presence of mature, elaunin and oxytalan fibres. An observation was made that a number of fibres appeared to ‘kink’ at their point of exit from the collagen bundle into the interlamellar space. This characteristic is illustrated by the circles in Figure 3.15d.

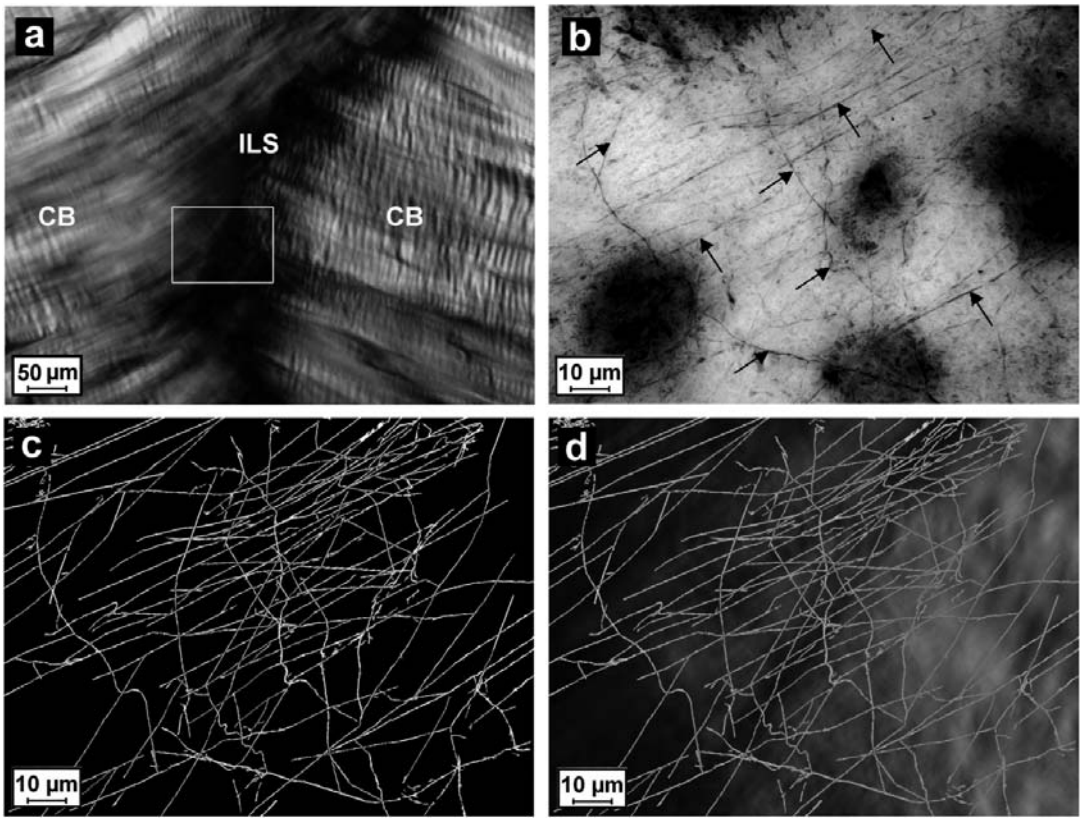


Figure 3.14. Interlamellar elastic fibres and the surrounding matrix architecture viewed in the lamellar plane (40 year old, grade 2 specimen). (a) Polarised light image depicting an oblique cut through the interlamellar space (ILS) separating two collagen bundles in consecutive lamellae (CB). (b) High magnification, phase contrast, z-series composite image in the region of image (a) indicated by the square, showing a complex meshwork of elastic fibres in the interlamellar space (examples indicated by arrows). (c) Binarised reconstruction of (b). (d) Elastic fibres in (c) are superimposed over a high magnification, cross-polarised light view of the same region.

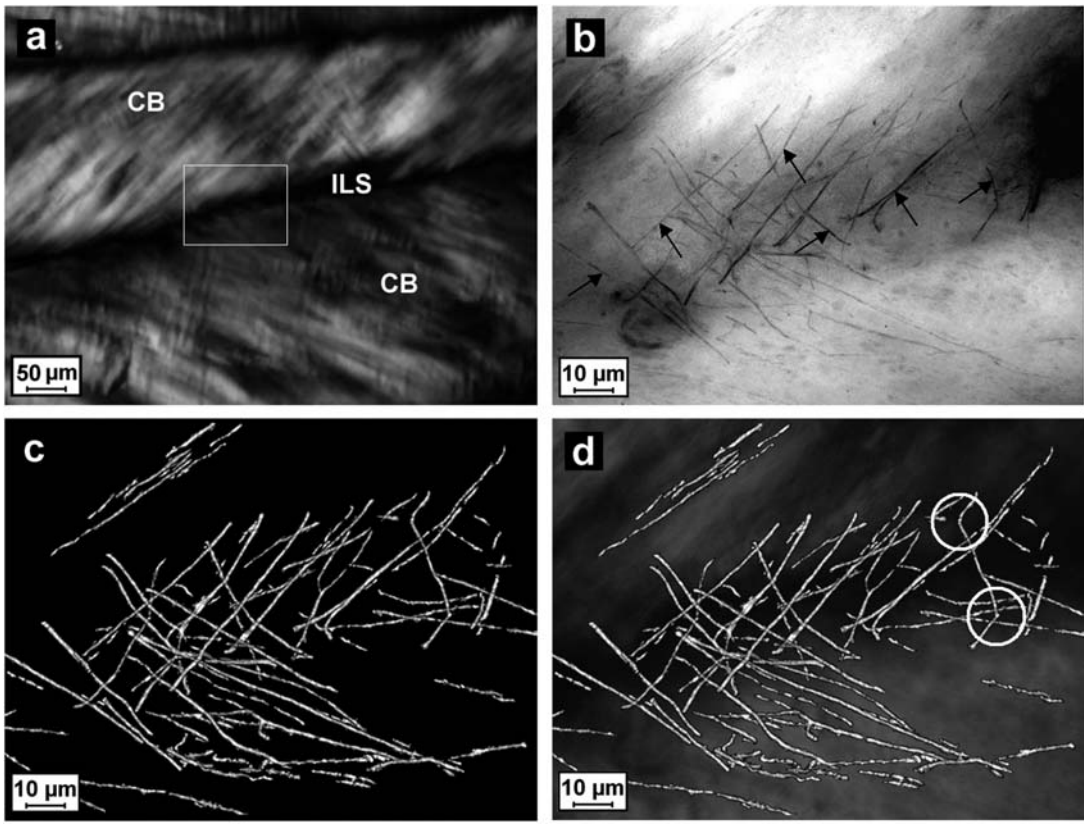


Figure 3.15. Interlamellar elastic fibres and the surrounding matrix architecture viewed in the transverse plane (54 year old, grade 2 specimen). (a) Polarised light image depicting two collagen bundle lamellae (CB) separated by an interlamellar space (ILS). (b) High magnification, phase contrast, z-series composite image in the region of image (a) indicated by the square, showing a complex meshwork of elastic fibres (examples indicated by arrows) in the interlamellar space. (c) Binarised reconstruction of (b). (d) Elastic fibres in (c) are superimposed over a high magnification, cross-polarised light view of the same region showing elastic fibre distribution relative to the collagen microarchitecture. The circles indicate apparent fibre ‘kinks’ at the points of anchorage into the collagen bundles.

3.6.5 Regional Variations in Intralamellar Elastic Fibre Density

Figure 3.8 is representative of those images used for the quantitative analysis. Individual results for each specimen are given in Table 3.2. Overall intralamellar elastic fibre density was significantly greater in the posterolateral region of the anulus than the anterolateral (AL = 6 ± 2, PL = 12 ± 4, p = 0.002, fibres per 100 microns, mean ± SD, AL = anterolateral, PL = posterolateral). Additionally, it was found that this circumferential variation was independent of radial location (outer: AL = 9 ± 3, PL = 17 ± 6, p = 0.001; middle: AL = 6 ± 2, PL = 12 ± 6, p = 0.02; inner: AL = 4 ± 2, PL = 6 ± 3, p = 0.007) (Figure 3.16). An F-test revealed that elastic fibre density variance was significantly greater within the posterolateral region than the anterolateral (p = 0.0003).

Single factor analyses of variance demonstrated that significant variations in intralamellar elastic fibre density occurred with radial location in both anterolateral (p = 0.006) and posterolateral (p = 0.002) regions (Figure 3.16). Pair-wise Bonferroni corrected p values indicated that in both circumferential regions, the lamellae of the outer anulus had a significantly higher elastic fibre density than the lamellae of the inner anulus (AL: p = 0.005; PL: p = 0.002). No significant differences were detected between outer and middle (AL: p = 0.09; PL: p = 0.2), and middle and inner regions (AL: p = 0.6; PL: p = 0.1).

While not stated specifically as an objective, and not validated statistically due to the small sample size, a number of observations were made with respect to variations in elastic fibre density with age: an increasing trend between the ages of 16 and 40 was

observed, followed by a marked decrease, with the exception of the 76 year old, which had an overall fibre density higher than both the 60 and 82 year olds.

Comprehensive data tables are provided in Appendix 3.

Age	AL* Outer	AL Middle	AL Inner	PL* Outer	PL Middle	PL Inner	Overall
16	7 ± 3	4 ± 1	2 ± 1	15 ± 3	7 ± 4	4 ± 1	6 ± 5
28	13 ± 5	8 ± 2	3 ± 2	22 ± 8	17 ± 2	5 ± 3	10 ± 8
40	10 ± 2	8 ± 3	6 ± 2	21 ± 7	20 ± 9	10 ± 2	12 ± 8
54	11 ± 2	7 ± 2	4 ± 2	21 ± 4	15 ± 3	6 ± 4	11 ± 7
66	8 ± 4	6 ± 3	4 ± 2	8 ± 5	9 ± 4	4 ± 2	7 ± 4
76	10 ± 2	4 ± 2	7 ± 1	22 ± 7	15 ± 4	9 ± 3	11 ± 7
82	3 ± 2	4 ± 1	3 ± 1	12 ± 6	2 ± 1	4 ± 2	5 ± 5

Table 3.2. Intralamellar elastic fibre density, summarised by region for each specimen - fibres per 100μm (mean ± SD, n ≥ 6). *AL = anterolateral, PL = posterolateral

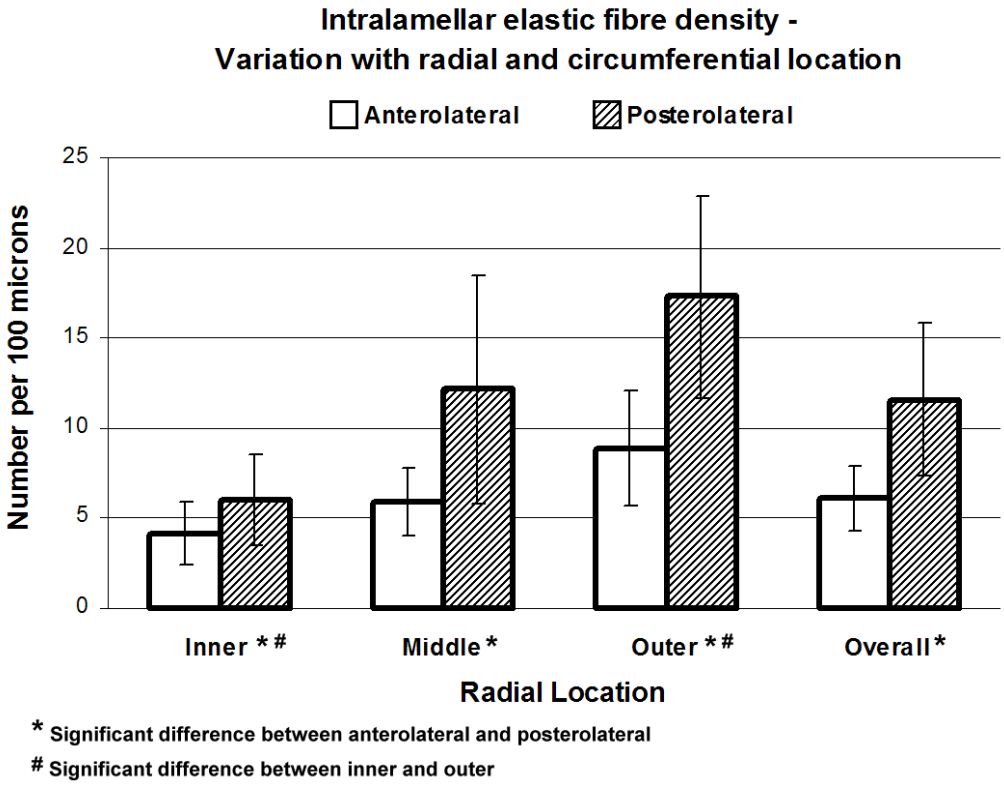


Figure 3.16. Variations in intralamellar elastic fibre density with radial and circumferential location, (mean ± SD, n = 7). Significance was detected between anterolateral and posterolateral (inner: p = 0.02, middle: p = 0.007, outer: p = 0.001, overall: p = 0.002), and between inner and outer (anterolateral: p = 0.005, posterolateral: p = 0.002).

3.7 Discussion

In this histological investigation, a quantitative description of the distribution of elastic fibres within the lamellae of each region in the human lumbar anulus fibrosus was presented, and a multi-planar comparison of elastic fibre distribution patterns in the intralamellar and interlamellar zones was described. The unique methodology developed allowed visualisation of elastic fibres in the anulus at a level of detail not previously achieved.

A number of previous histological studies of the anulus fibrosus elastic fibre network have used enzymatic degradation of collagen and glycosaminoglycans to enhance visibility (Yu *et al.*, 2002; Yu *et al.*, 2005; Yu *et al.*, 2007). It was noted in these studies that without this pre-treatment, elastic fibres were masked to an extent by the surrounding matrix. Given the close association observed between elastic fibres and collagen in particular, it is plausible that such pretreatment could significantly alter the overall matrix structure, and in consideration of those changes which may have already occurred due to freezing, fixation and processing, pretreatment was therefore not undertaken. Masking of elastic fibres by the surrounding matrix was largely overcome using the novel imaging techniques described; it is possible that such masking, taken in combination with isolated heavy background staining, may have resulted in overall underestimation of the total number of elastic fibres. While such underestimation may be important in the context of determining overall elastic content, it would be unlikely to confound the results of a comparative study such as the one described here.

A comparison of elastic fibre distribution patterns in intralamellar and interlamellar zones performed at high magnification in the lamellar and transverse planes revealed differences which suggest that elastic fibres convey unique functionality at multiple levels of the anulus structural hierarchy, and support a rejection of the third null hypothesis proposed at the chapter outset. Within lamellae elastic fibres were observed to be closely associated with the surrounding collagen matrix, corresponding well to previous observations in the transverse plane (Buckwalter *et al.*, 1976; Johnson *et al.*, 1984; Yu *et al.*, 2002; Yu *et al.*, 2005). Additionally, fibres appeared not to be confined to the collagen bundle peripheries. Planar crimping of fibrous collagen, as has been well documented (Cassidy *et al.*, 1989), was clearly observed, particularly in lamellar plane sections. Elastic fibres appeared to conform to the crimp pattern of the surrounding collagen (Figure 3.12), and their close association with collagen more generally suggest that the overall mechanical response of the matrix is a product of their mutual interaction, in addition to the interactions which may occur with proteoglycans.

In interlamellar zones, elastic fibres appeared in structurally complex three-dimensional meshworks, which branched out across lamellar interfaces. Combinations of both very large and very fine fibres were observed in these meshworks, suggesting the presence of all three elastic fibre types (mature, elaunin and oxytalan). It is possible either that these fibres are various stages of development, or are fully developed and convey unique functional capabilities. Results suggest that the complex linkages previously observed between collagen bundles in adjacent lamellae (Pezowicz *et al.*, 2006a) are indeed, at least partially, composed of elastic fibres. A number of fibres were seen to ‘kink’ at their point of exit from the collagen bundle

into the interlamellar space, suggesting that the collagen bundles on either side of the interlamellar space into which the ends of elastic fibres are anchored have undergone relative movement, providing further evidence that these fibres function as mechancial links between lamellae. One possible explanation for the relative structural complexity of elastic fibres at lamellar interfaces may be the fact that the two populations of collagen fibres with which they appear to integrate on either side of the interface are oriented in opposite directions; this contrasts with the relatively uni-directional alignment of those elastic fibres within the lamellae, which are integrated with collagen fibres that have a single preferential alignment.

Quantitative analysis revealed intralamellar elastic fibre density to be significantly higher in the posterolateral region of the anulus than the anterolateral, and significantly higher in the outer regions of the anulus than the inner, supporting a rejection of the first and second null hypotheses proposed at the chapter outset. To gain insights into why these differences in matrix structure may exist, consideration can be given the types of strains to which lamellae in different regions of the anulus are exposed during normal daily activity. During flexion, the posterior regions of the L3-L4 anulus experience positive axial strains of up to 60 percent, in contrast to the anterior regions, which experience just 3 percent in extension (Pearcy and Tibrewal, 1984). Additionally, in torsion, surface strains in the collagen fibre bundles of the posterolateral region exceed those in the anterior region by a factor of two to one (Stokes, 1987). Associated strains under the above loading conditions are greater in the collagen fibre bundles of the outer lamellae due to their relative distances from the axes of movement. It can hence be hypothesized that elastic fibre density is positively correlated with the magnitudes of the tensile deformations experienced by different

regions of the anulus under these loading conditions. An analysis of elastic fibre distribution in the flexor tendon, a comparable tissue, has suggested a similar correlation between elastic fibre distribution and strain magnitude (Ritty *et al.*, 2002).

Although there are currently no experimental biomechanical data describing the functional roles played by elastic fibres in the mechanics of the intervertebral disc, their role has been described in a number of other comparable tissues, discussed in section 1.2.2.3 (Karlinsky *et al.*, 1976; Oakes and Bialkower, 1977; Oxlund *et al.*, 1988; Brown *et al.*, 1994; Lee *et al.*, 2001). The results of these studies suggest that a primary function of elastic fibres in the anulus would be to limit and reverse distention of the collagen matrix in the locations they have been observed, i.e. both in the intralamellar zones between fibrils and bundles, and at interlamellar zones by connecting bundles in adjacent lamellae. These questions are addressed in Chapters 4 and 5.

The small number of cases did not permit a statistically valid analysis to be conducted into elastic fibre density variation with age. Indeed, the potentially large sample size that would be required for such a study and the time consuming nature of the analytical methodology used here placed it outside the scope of this project. Accepting that any conclusions made regarding such correlations should be treated with caution for this reason, a number of observations made from the values presented in Table 3.2 are worthy of discussion. Results show an increasing trend in intralamellar elastic fibre density between the ages of 16 and 40, followed by a decrease, with the exception of the 76 year old, which had an overall fibre density higher than both the 60 and 82 year olds. A comparison of disc dimensions, disc morphological grades and vertebral body bone mineral densities for the 60, 76 and 82

year old specimens revealed that while all were assigned a grade of 3, the 76 year old specimen had reduced height, as well as a significant mismatch in bone mineral densities (T-scores) between the superior (L3) and inferior (L4) vertebral bodies (Table 3.1). These factors could be reasonably be expected to result in altered mechanical behaviour for this disc and, hence, matrix composition. Additionally, of these three the 76 year old was the only female. If this specimen is excluded for the reasons described, the results appear broadly consistent with existing biochemical data showing that the elastin content of the anulus increases from birth until the age of 40, then steadily decreases (Olczyk, 1994). They are given added significance by recent findings that the tensile deformability of human lumbar discs peaks between the ages of 31 and 40, and subsequently decreases (Kurutz, 2006). Further work is required to confirm this apparent correlation. Interestingly, a more recent study suggests that elastin content increases with degeneration – in the context of the trends observed here, it is possible that this increase is localised in regions other than the intralamellar.

There were several limitations to this study: no assessment was made of the effect of distance from the endplates and vertebral bodies on elastic fibre density, although every effort was made to ensure sections were taken close to the mid-plane of the disc; aqueous fixation may have resulted in some distortion of lamellae, particularly in the inner anulus where glycosaminoglycan content is higher; the effects of freezing and fixation on aspects of tissue morphology such as collagen fibril arrangement, and, consequentially, elastic fibre arrangement, were not assessed, however, the results of a previous study suggest that such effects would be unlikely to significantly influence the results (Hickey and Hukins, 1979). Despite the robust imaging and quantitation

methodology used, occasional heavy background staining may have resulted in some fine elastic fibres being obscured.

In light of the findings presented, any decrease in elastic fibre density with age or pathology is of potential clinical significance, particularly with respect to those regions of the anulus subjected to the highest and most frequent deformations such as the posterior and posterolateral, which are also the most frequent sites for degenerative changes such as radiating tears (Vernon-Roberts *et al.*, 1997). Additionally, weakening of those elastic fibres which bridge the interlamellar spaces could make the anulus more susceptible to delamination and the formation of circumferential lesions.